ESI

Content

A.Experimental Procedures

Materials. Reagents were obtained from commercial sources and used without further purification. Perylene, C-(1,1-Dimethylethyl) N-(4-boronophenyl)carbamate, C-(1,1-Dimethylethyl) N-[(4-boronophenyl)methyl]carbamate, 3-Pyrrolidinamine, 2,6-Pyridinedicarbonyl dichloride, hydrochloride (1:2), Tricyclo[3.3.1.13,7]decane-1-methanamine, 1-(2-Naphthyl)ethylamine, 1-Aminoindan, and 3-Amino-1-butanol were purchased from Bide pharm. And other reagents were purchased from Shanghai Xiensi Biotechnology Co., Ltd. All solvents were reagent grade. All water used in this work was deionized (DI) water.

Instrumentation ^{1}H NMR spectra, ^{13}C NMR, ^{19}F NMR spectra were obtained by BRUKER AVANCE III HD 400. High-Resolution Mass Spectra (HR-MS) were performed on an Agilent Q-TOF 6510. Circularly polarized luminescence (CPL), Circular dichroism (CD), temperature-variable CD were measured with an Applied Photophysics ChirascanV100 model. Fluorescence lifetime was measured by Steady State-Transient-Fluorescence Spectrometer (Edinburgh FLS920). UV-Visible absorption spectra at room temperature were recorded on a UV-1900 Shimadzu spectrophotometer. Fluorescence spectra was made on a RF-6000 Shimadzu fluorophotometer. Scanning electron microscope (SEM) images were measured by a Zeiss scanning electron microscope (Germany). Transient absorption spectra were collected by Femtosecond Transient Absorption Spectrometer (Ultrafast, Helios, USA). An Astrella Ti: Sapphire laser system from Coherent Astrella (USA) was used as a light source. The ~70 fs pump laser pulse was generated by a regenerative amplifier system and the optical parametric amplifier (OPerA-Solo). The instrument

used for SAXs is the Xenocs in-house X-ray scattering beamline, model Xeuss 3.0 (France).

Assembly methods Unless otherwise stated, all assembly methods in this article follow the described procedure. Assembly behavior were explored in mixed solvents ($MeCN/H_2O$ = 2/8, v/v, 0.05mM) through a nanoprecipitation method. Testing should be conducted immediately after the solution is prepared. For solid testing, after preparation, the sample should be subjected to ultrasound at 50°C for 30 minutes and then aged for 24 hours. Any precipitate that forms should be collected, dried, and then tested.

Quantum mechanical calculation The structures of the host and guest molecules were optimized using the B3LYP-D3(BJ)/6-311G(d,p) basis set in the Gaussian 16 program to obtain low-energy conformations, from which their ESPs were derived. The results of IRI were obtained from the above optimized structure by Multiwfn.[S1,S2] The Antechamber program was used to fit the restrained electrostatic potential (RESP) charge, and then the general Amber force field (GAFF) was adopted to parameterize the for subsequent MD simulations. The topology files of molecules were parametrized under the corroboration of the GROMACS force field using Amber, ACPYPE, and Guassian tools.

Fitting method Benesi-Hildebrand plots was employed for fitting the absorption and fluorescence titration data. [S4] First, we performed the fitting calculations to obtain the binding constants using the following equation:

$$\frac{1}{A - A_0} = \frac{1}{P_1} + \frac{1}{P_1 P_2 C}$$

where A represents the absorbance, A_0 is the absorbance of the host molecule itself, C is the concentration of the guest molecule, and P_2 is the binding constant. Then, the Gibbs free energy (ΔG) was calculated using the following equation:

$$\Delta G = -RT\ln K$$

where K is standard binding constant, R is the universal gas constant (8.314 $J \cdot mol \cdot K^{-1}$) and T is the temperature in Kelvin.

In our system, unlike traditional host-guest interactions such as conventional macrocycles, the present interactions exhibit multi-site and multi-faceted characteristics, akin to the behavior of cocrystals. The changes in the absorption spectra are caused by the AP driven coassemblies. Due to the strong aromatic packing tendency of perylenes, the absorption coefficients are rather low, which shall be significantly enhanced after the insertion of AP donors, behaving as the molecular barriers. And the AP complexation, in some cases, might not fully strictly followed the specific stoichiometry. Although the MS data show the presence of 1:1 binding stoichiometry, the progressive addition of excess AP donors might afford block-coassembly type aggregation that beyond the 1:1 binding ratio. Therefore, we believe for this reason, some of the fluorescence or absorption titration did not obey the fine fitting tendency.

B. Additional experimental data

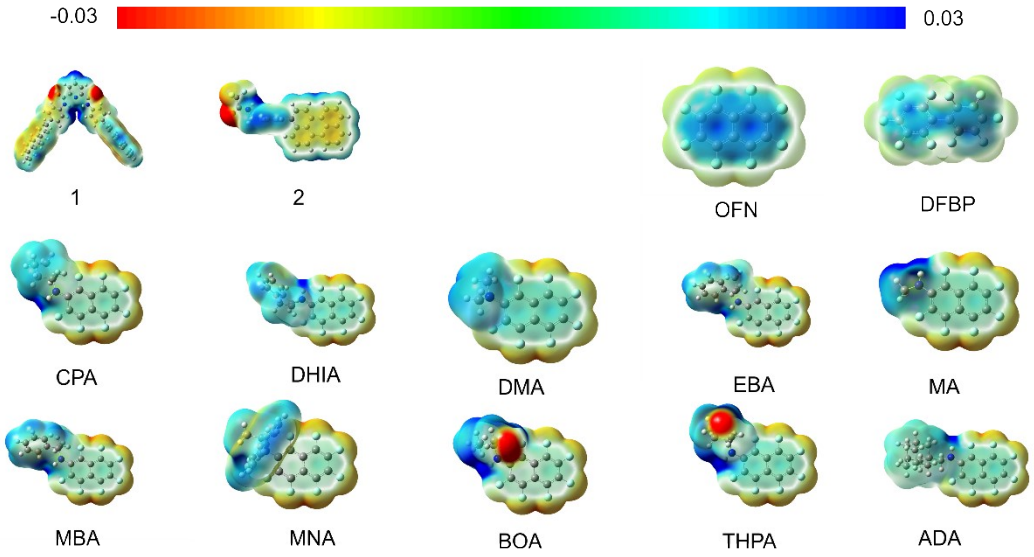

Figure S1. The electrostatic potential maps (ESP) of each molecule.

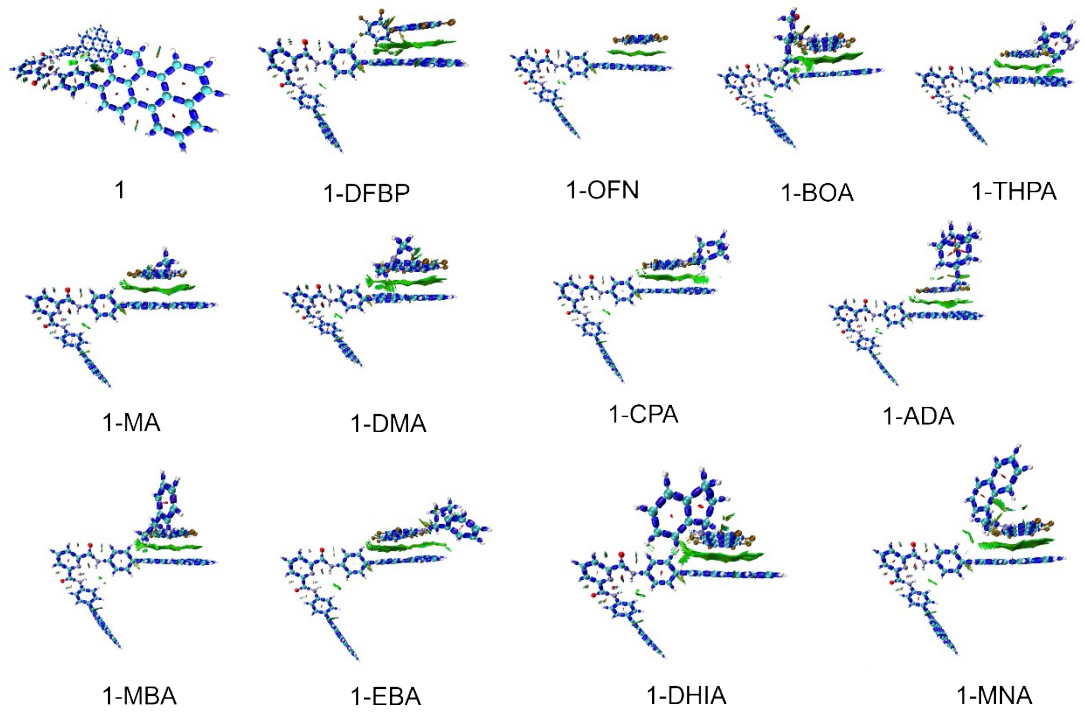

Figure S2. The Interaction Region Indicator (IRI) map of system with **1**.

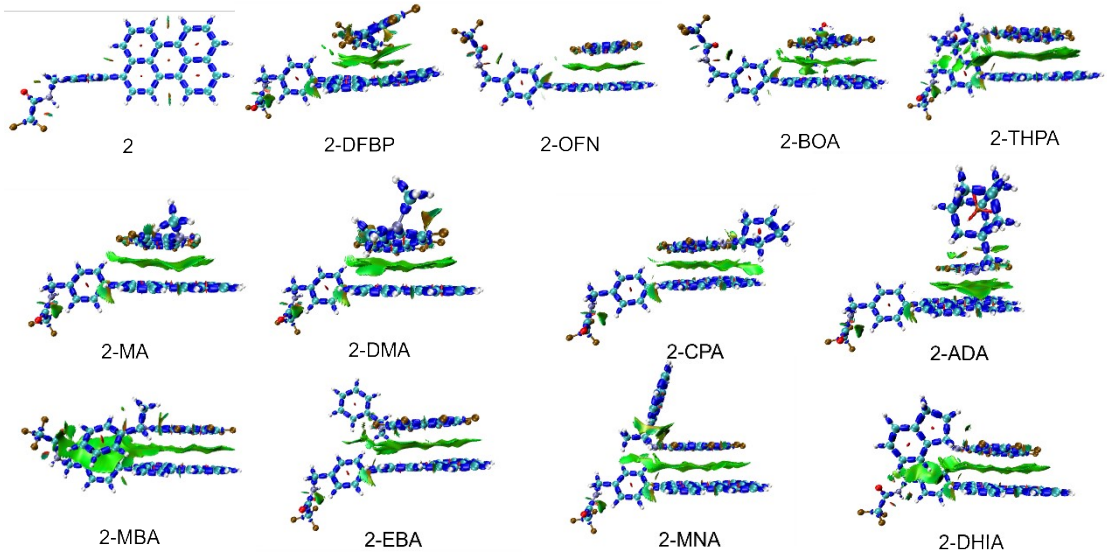

Figure S3. The Interaction Region Indicator (IRI) map of system with **2**.

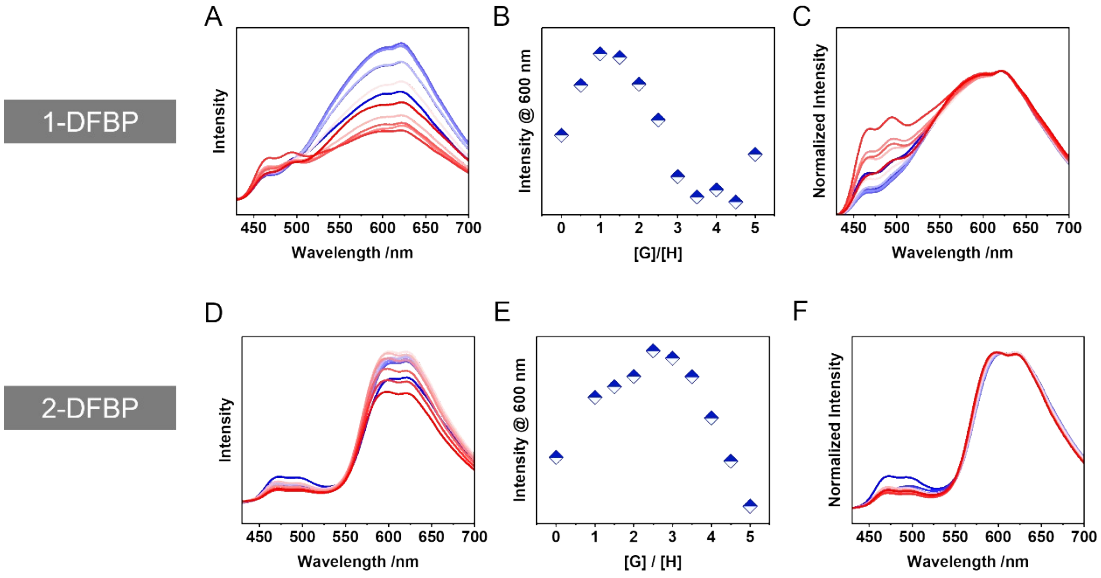

Figure S4. Fluorescence titration curves and normalized curves for the two hosts using DFBP.

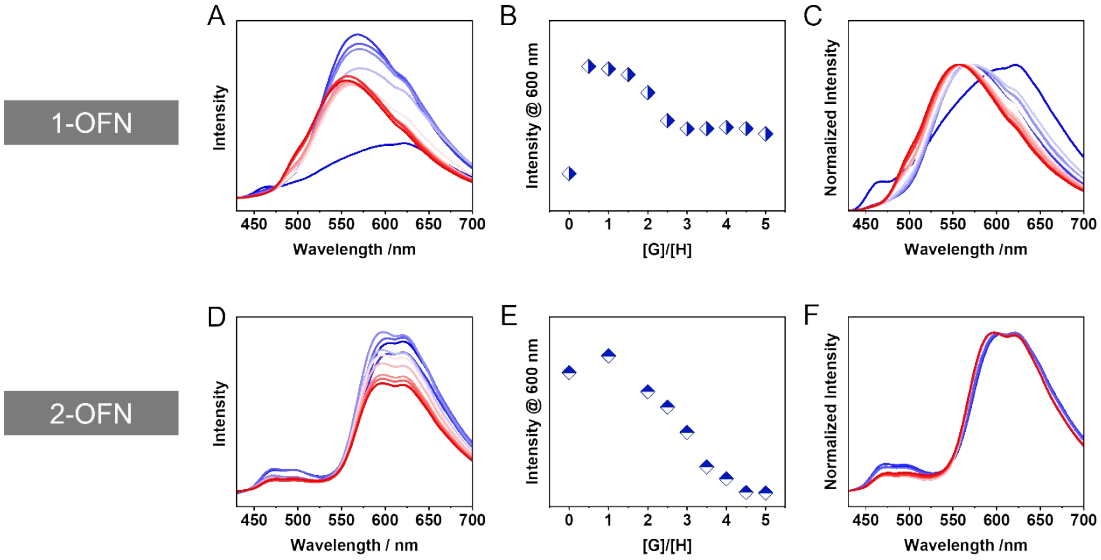

Figure S5. Fluorescence titration curves and normalized curves for the two hosts using OFN.

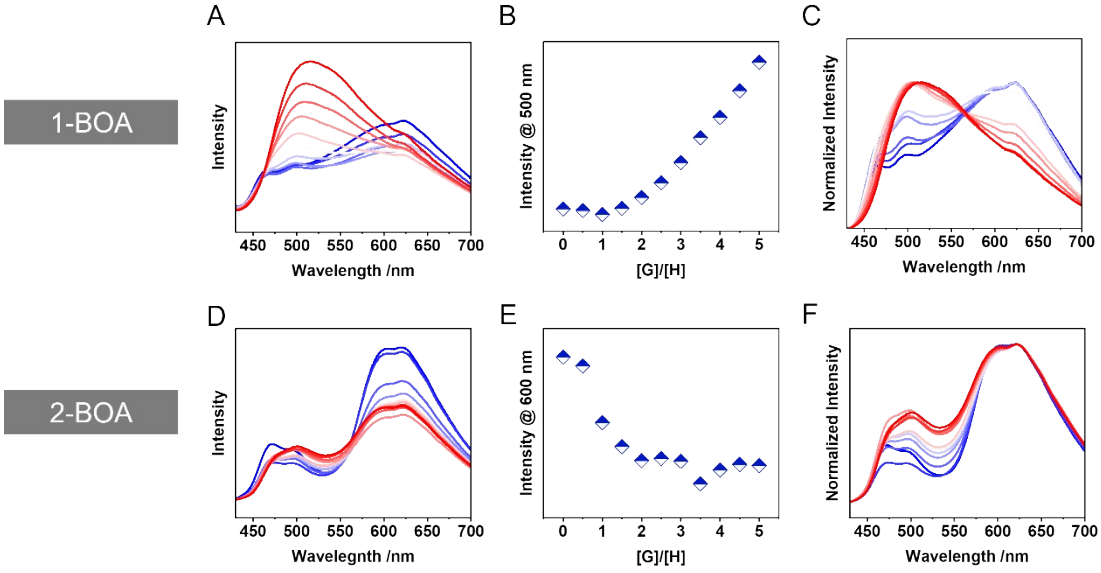

Figure S6. Fluorescence titration curves and normalized curves for the two hosts using BOA.

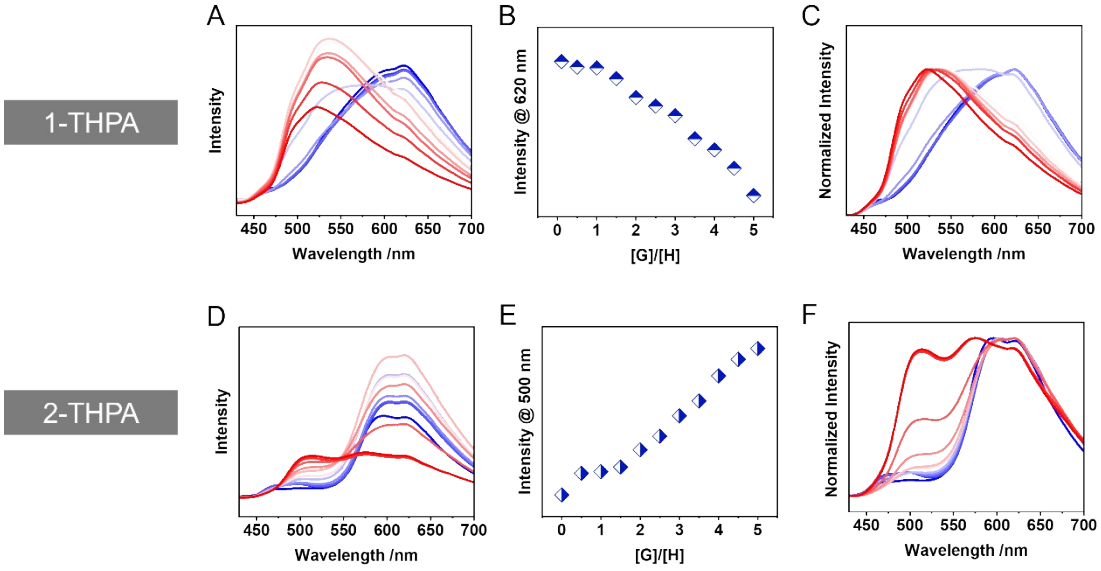

Figure S7. Fluorescence titration curves and normalized curves for the two hosts using THPA.

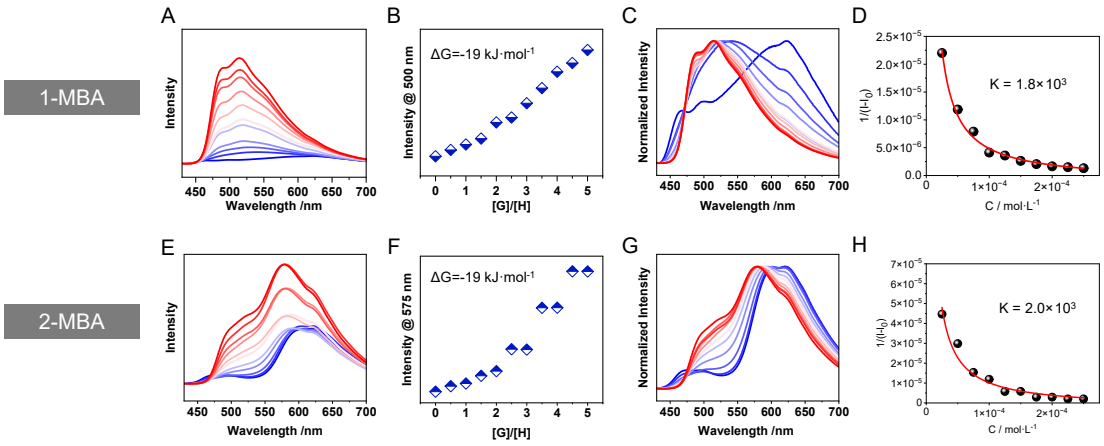

Figure S8. Fluorescence titration curves, normalized curves and fitting curves for the two hosts using MBA. (The standard binding constant was given in the figure, as well as the Gibbs free energy values obtained from fitting these data.)

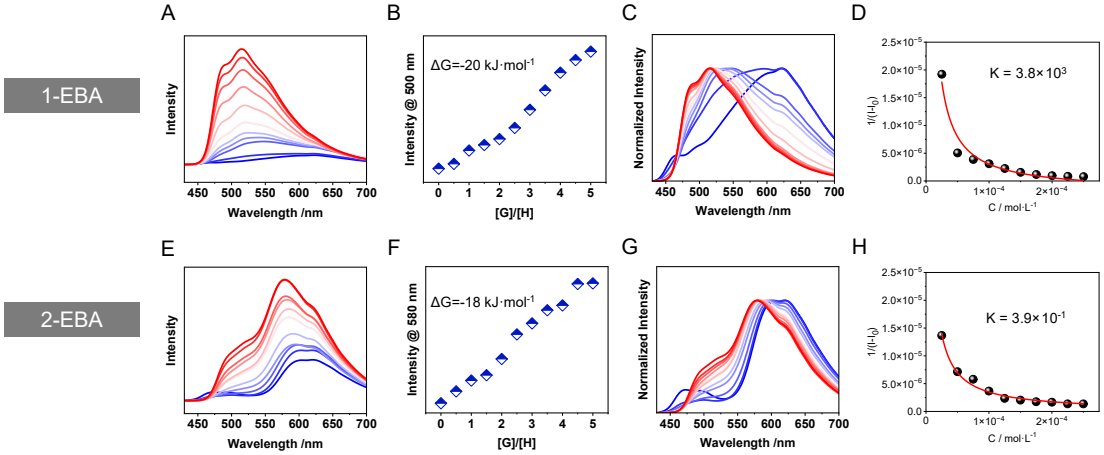

Figure S9. Fluorescence titration curves, normalized curves and fitting curves for the two hosts using EBA.

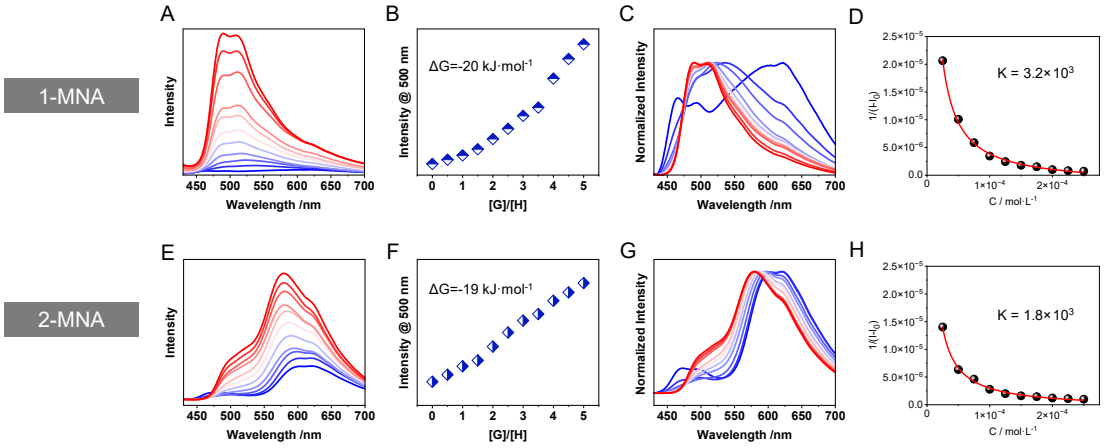

Figure S10. Fluorescence titration curves, normalized curves and fitting curves for the two hosts using MNA.

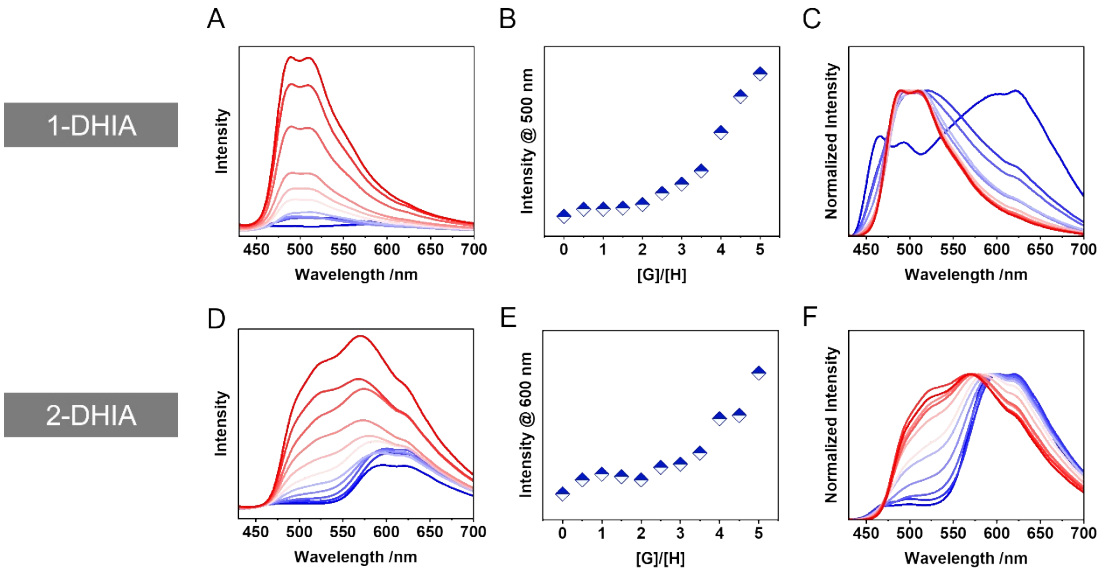

Figure S11. Fluorescence titration and normalized curves for the two hosts using DHIA.

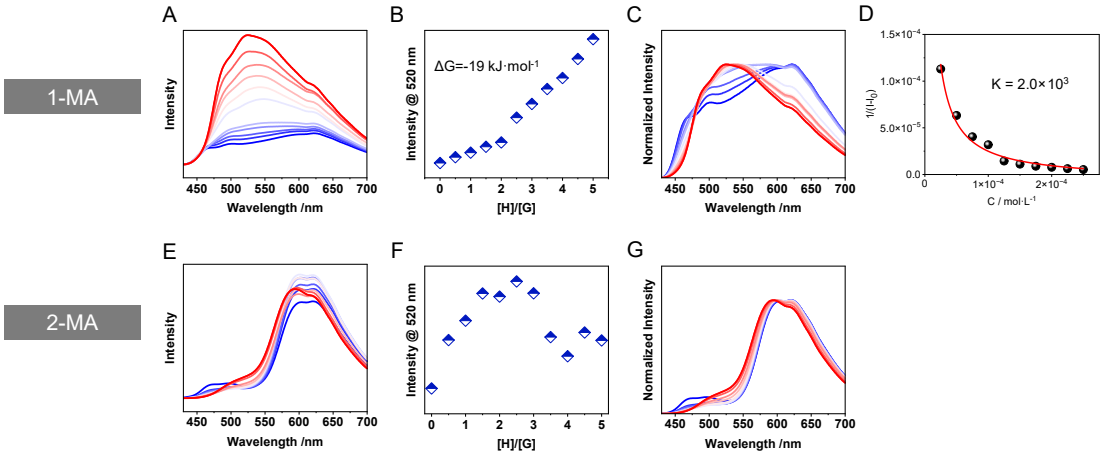

Figure S12. Fluorescence titration curves, normalized curves and fitting curves for the two hosts using MA.

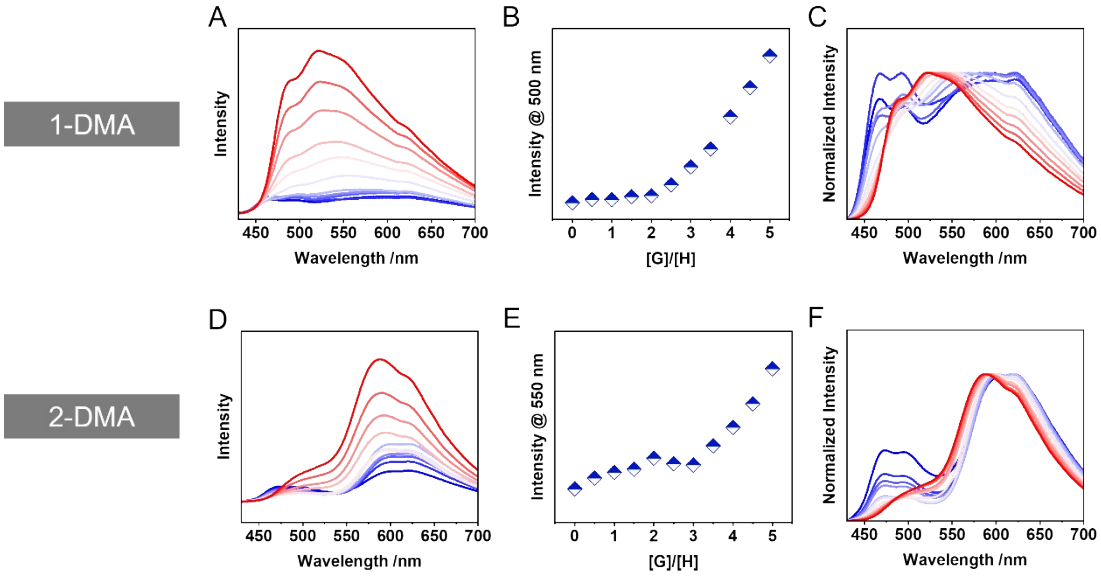

Figure S13. Fluorescence titration curves and normalized curves for the two hosts using DMA.

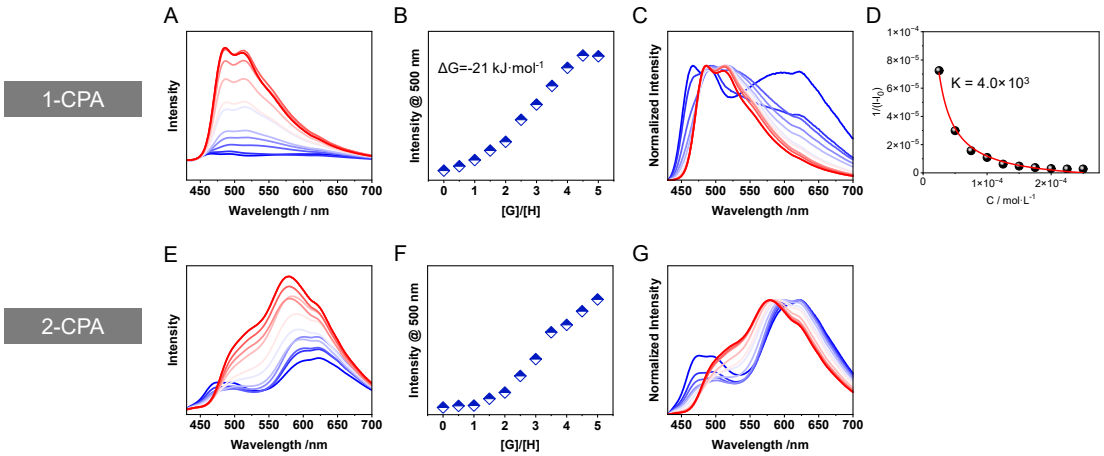

Figure S14. Fluorescence titration curves, normalized curves and fitting curves for the two hosts using CPA.

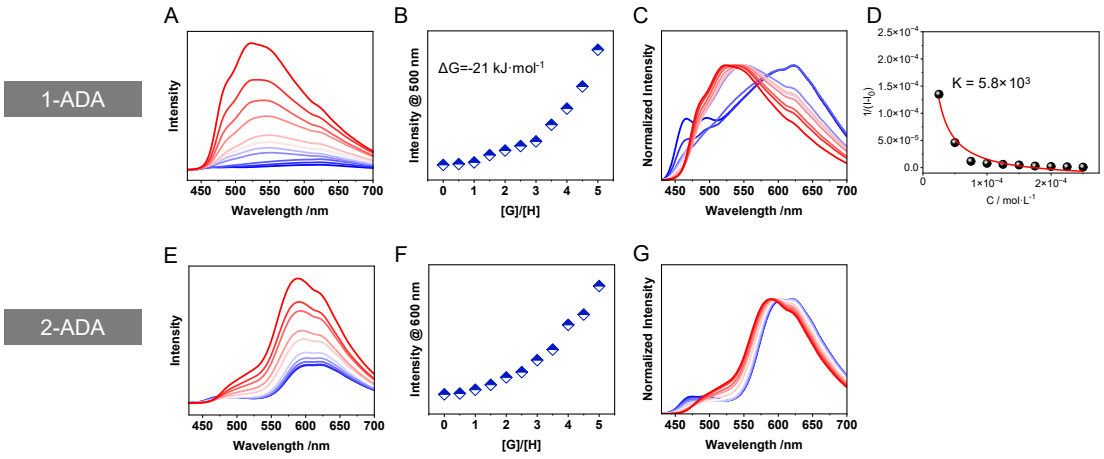

Figure S15. Fluorescence titration curves, normalized curves and fitting curves for the two hosts using ADA.

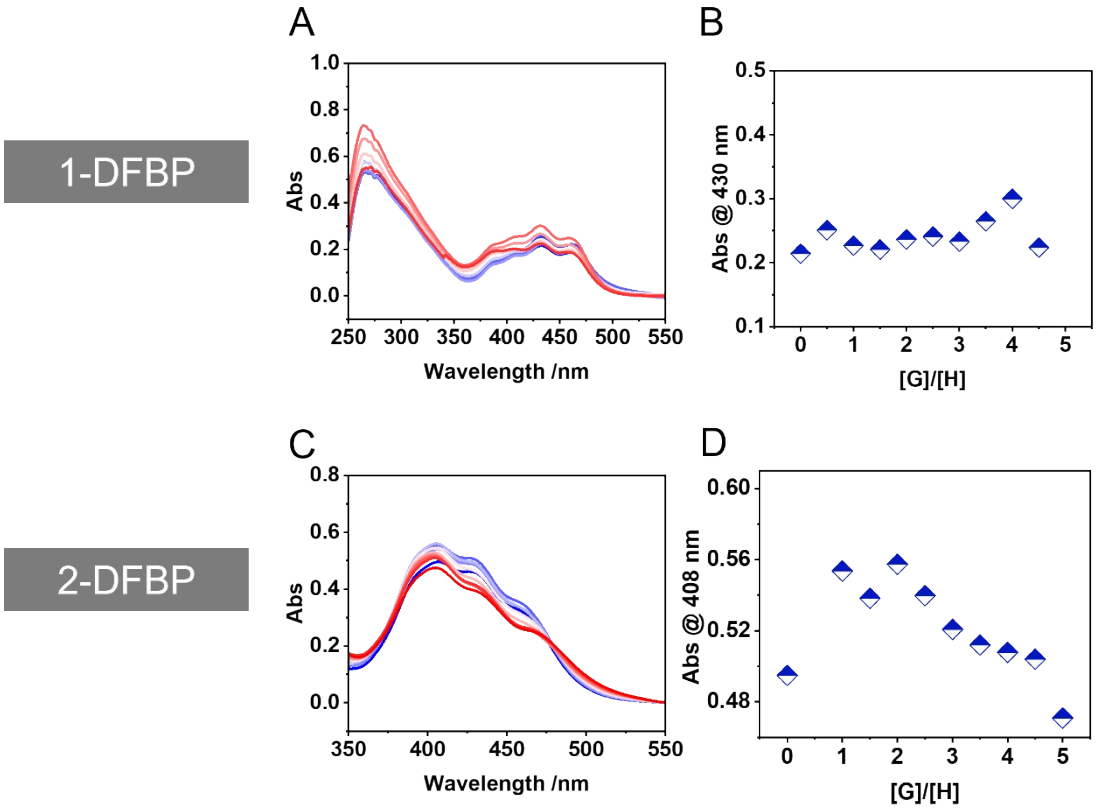

Figure S16. UV titration curves and normalized curves for the two hosts using DFBP.

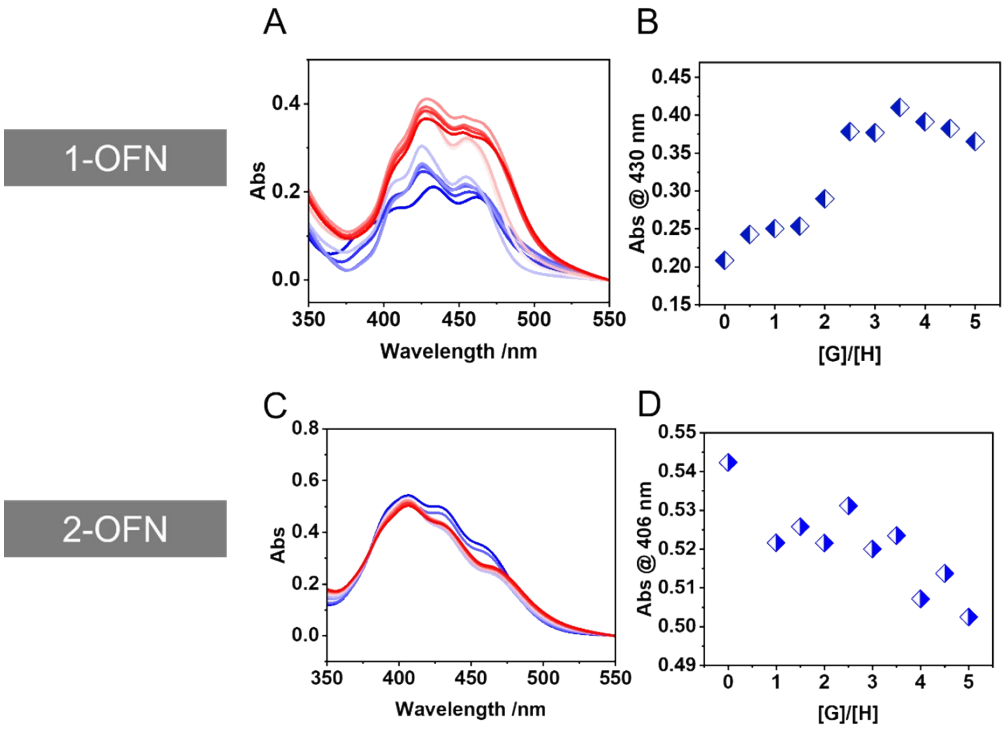

Figure S17. UV titration curves and normalized curves for the two hosts using OFN.

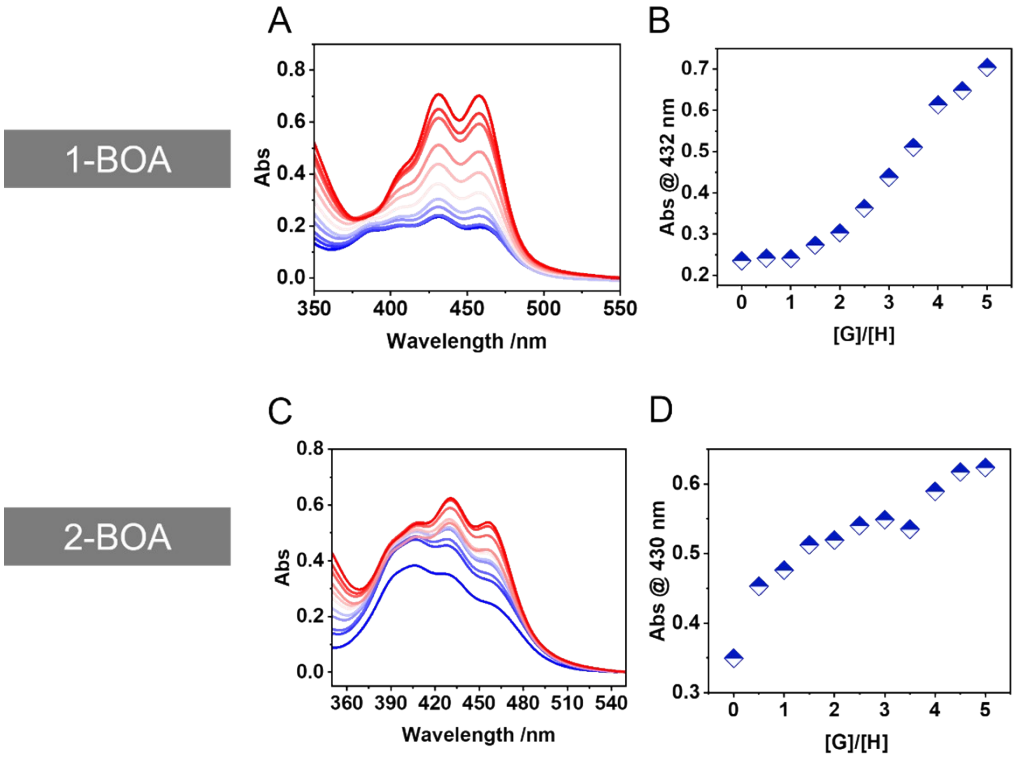

Figure S18. UV titration curves and normalized curves for the two hosts using BOA

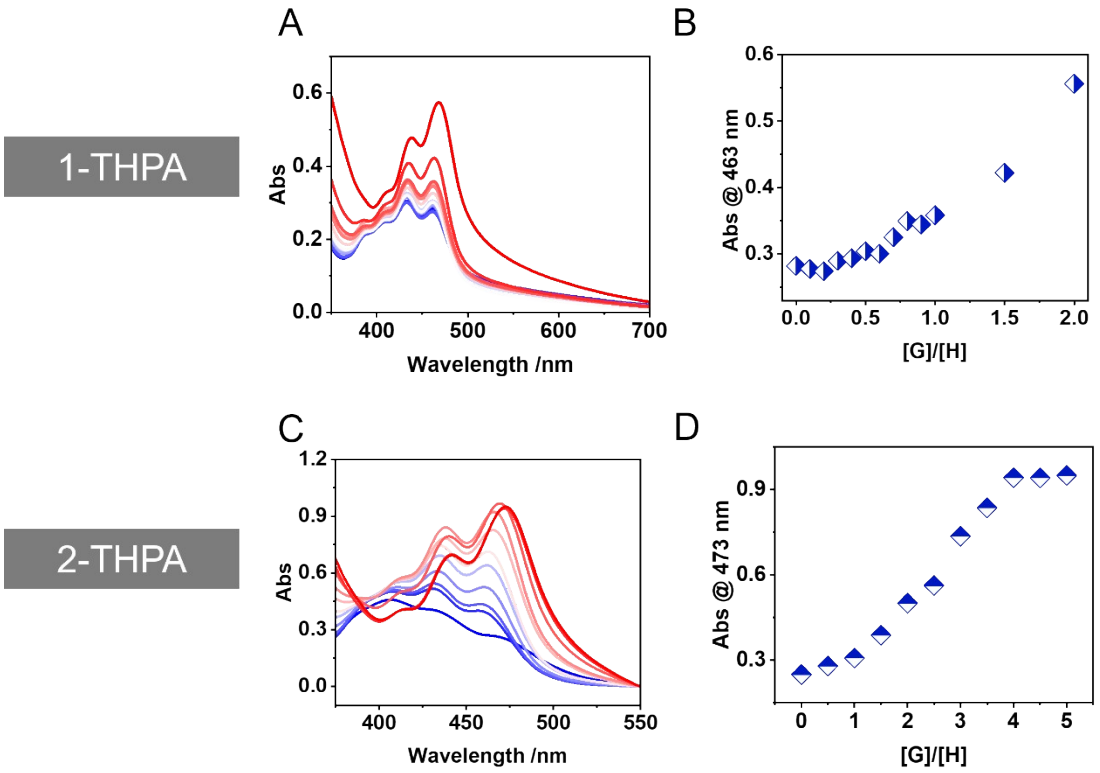

Figure S19. UV titration curves and normalized curves for the two hosts using THPA.

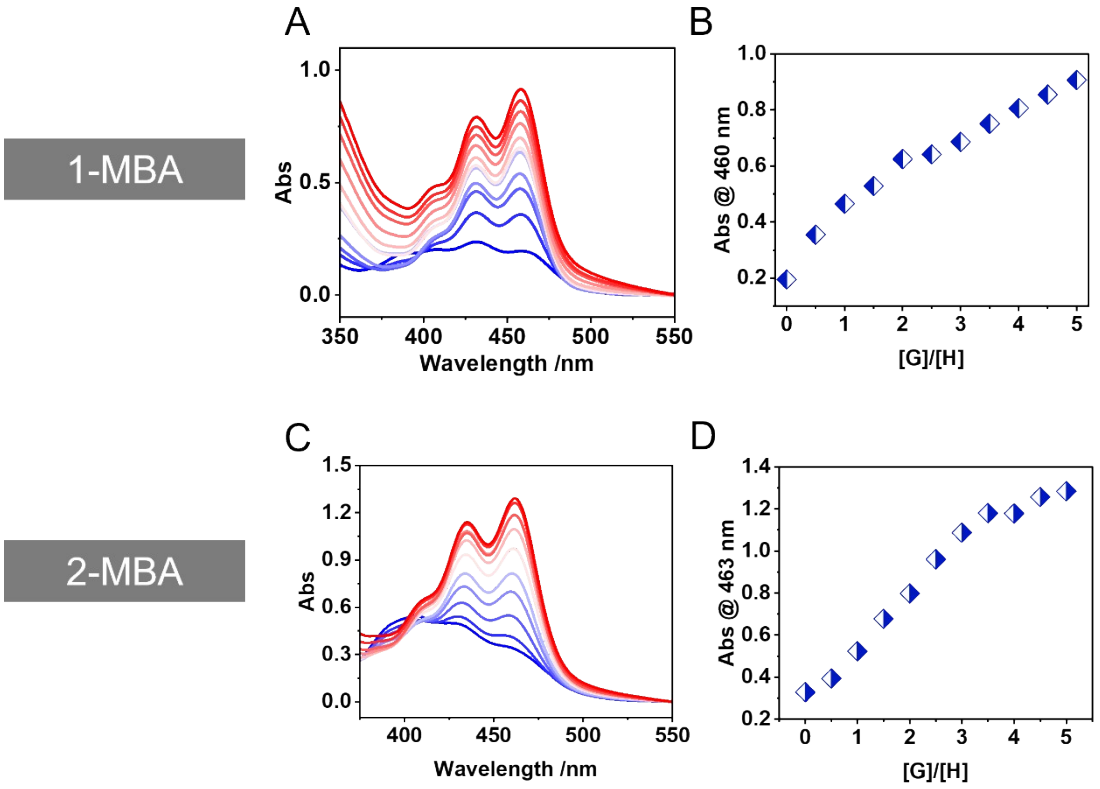

Figure S20. UV titration curves and normalized curves for the two hosts using MBA.

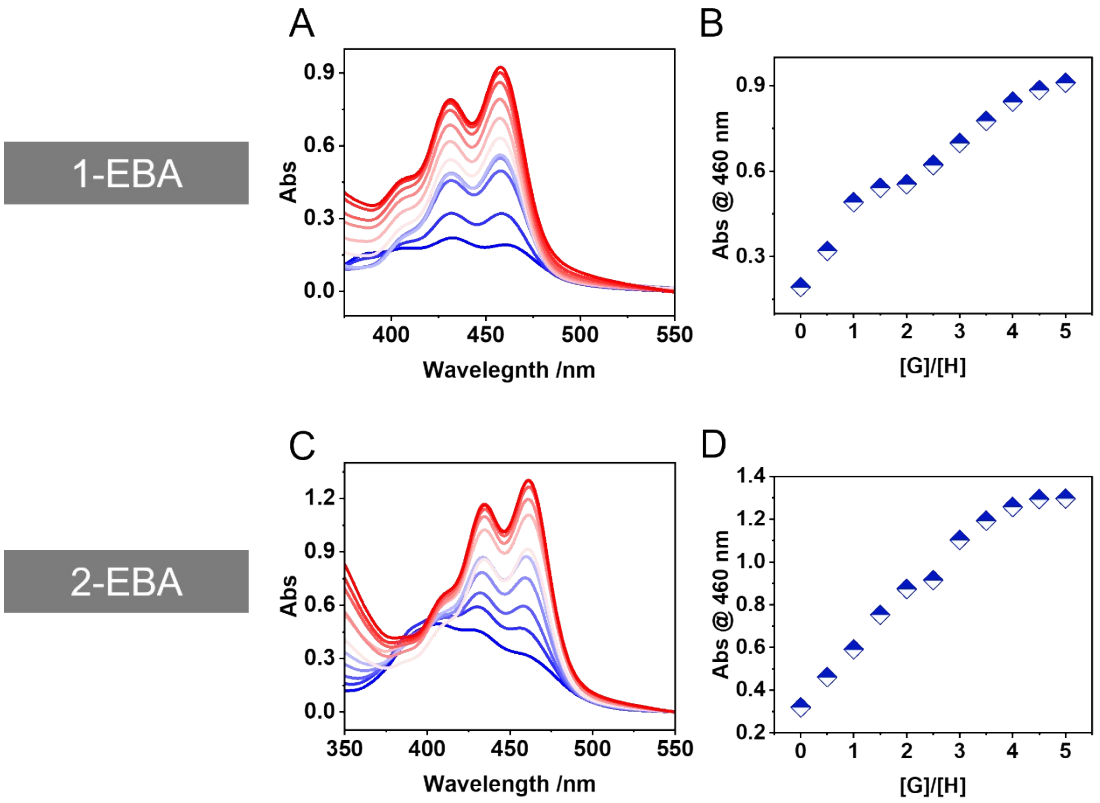

Figure S21. UV titration curves and normalized curves for the two hosts using MBA.

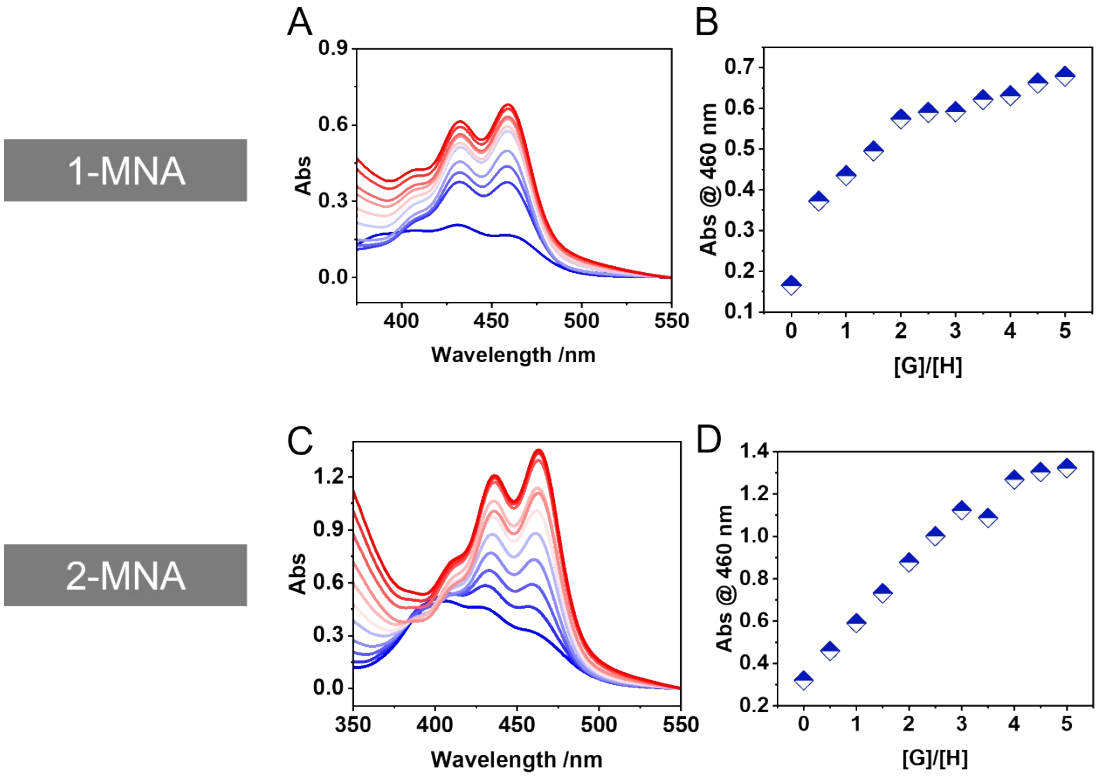

Figure S22. UV titration curves and normalized curves for the two hosts using MBA.

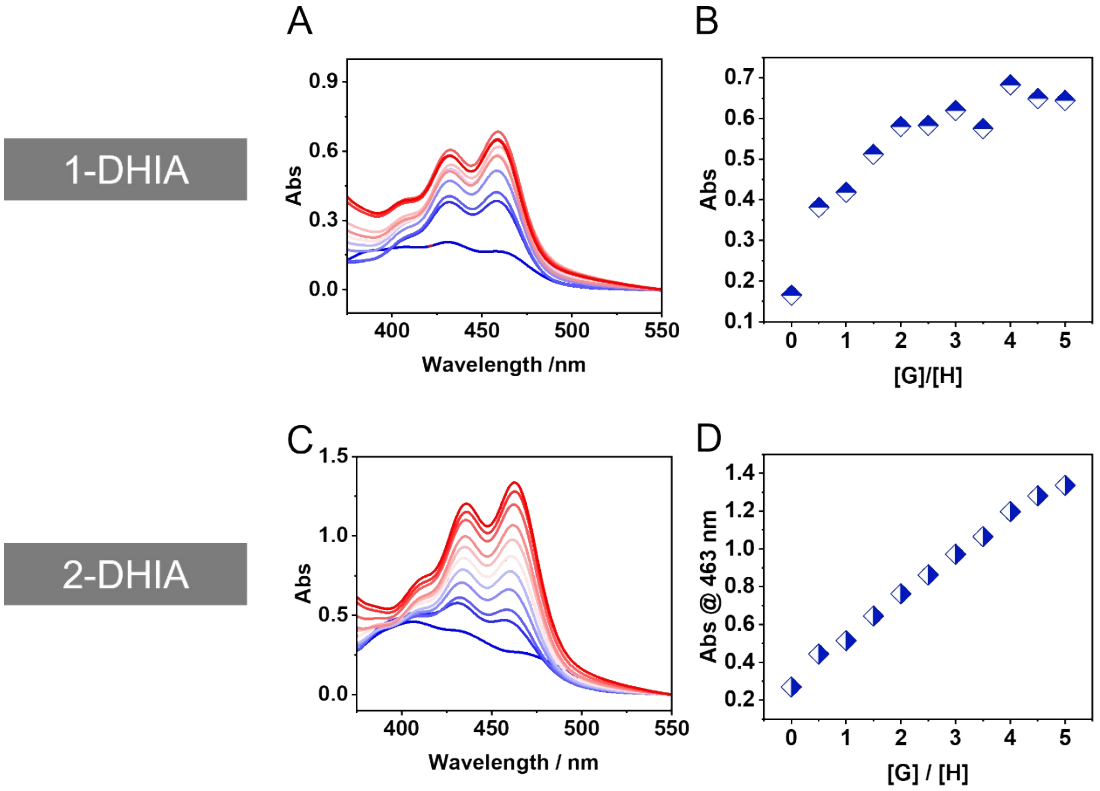

Figure S23. UV titration curves and normalized curves for the two hosts using DHIA.

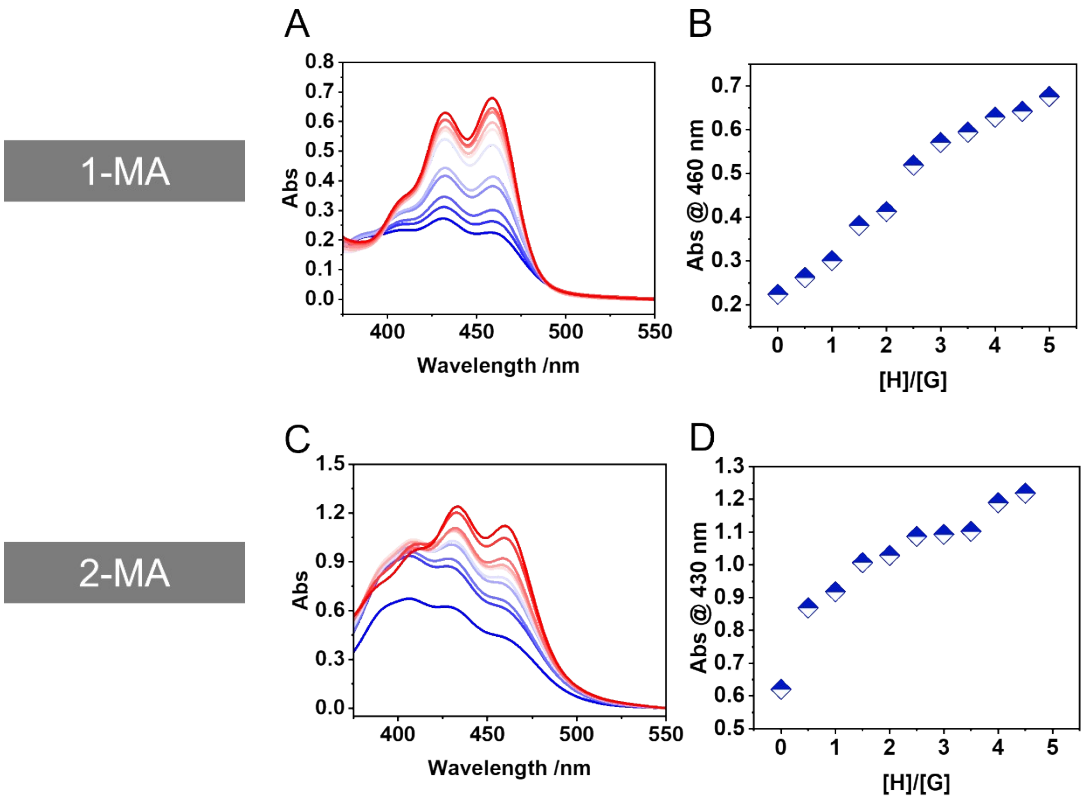

Figure S24. UV titration curves and normalized curves for the two hosts using MA.

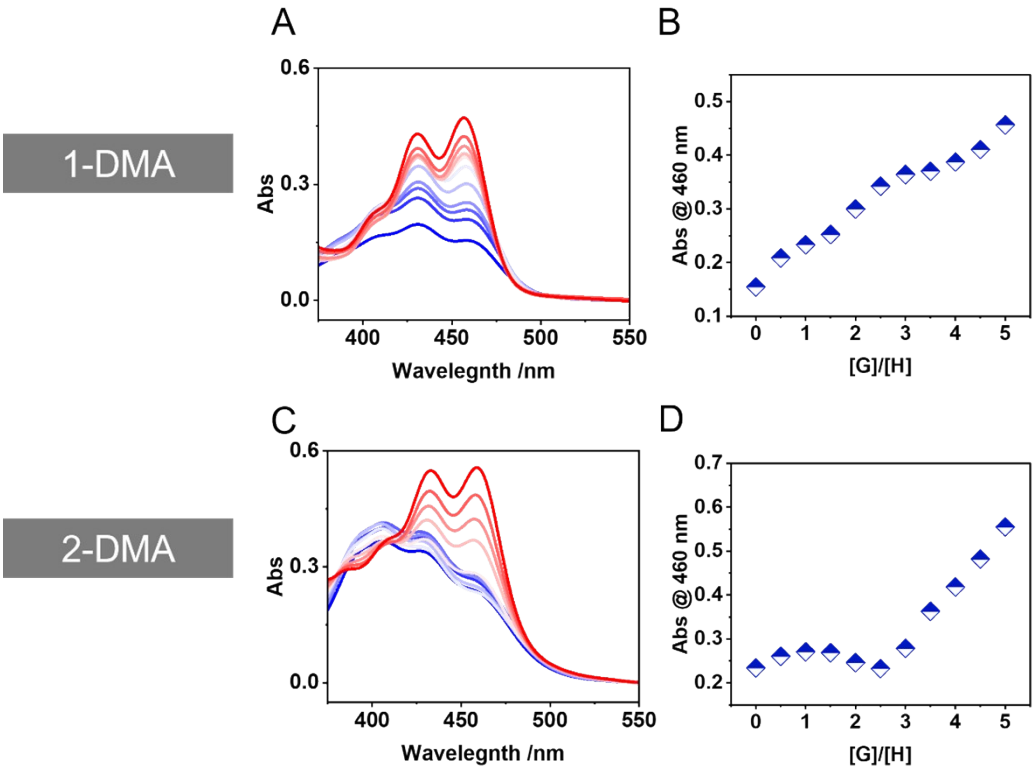

Figure S25. UV titration curves and normalized curves for the two hosts using DMA.

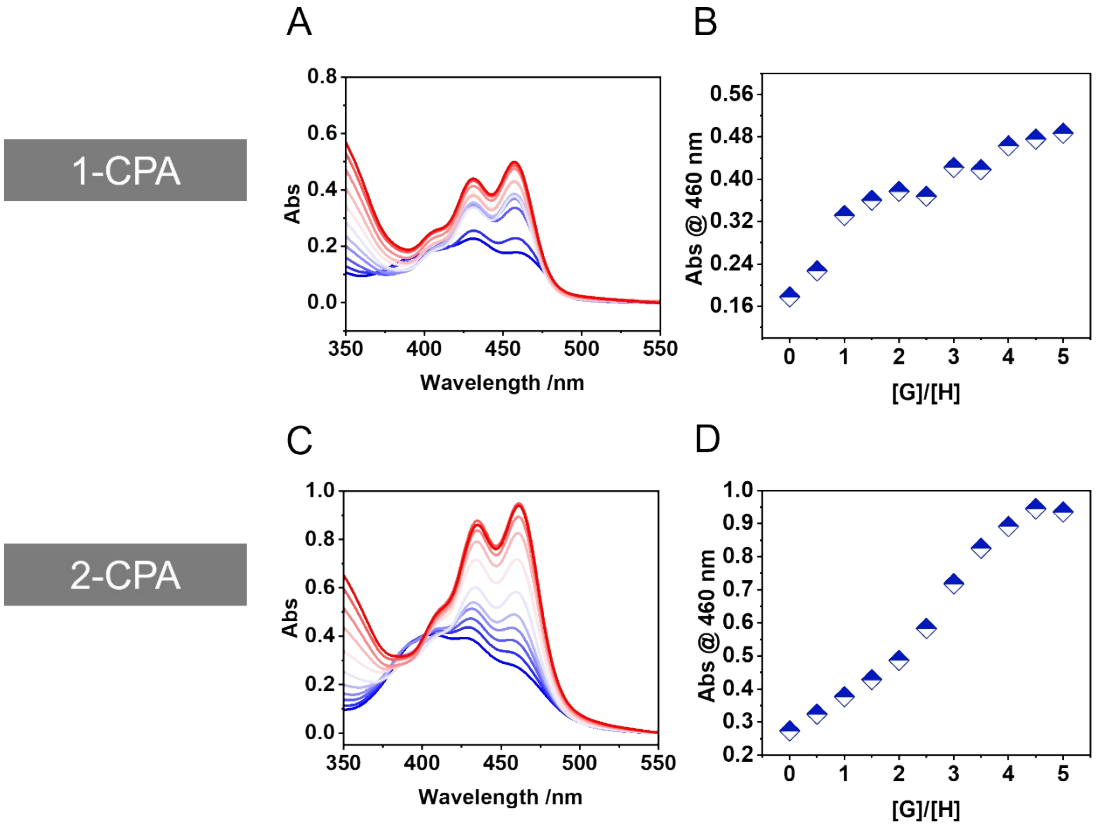

Figure S26. UV titration curves and normalized curves for the two hosts using CPA.

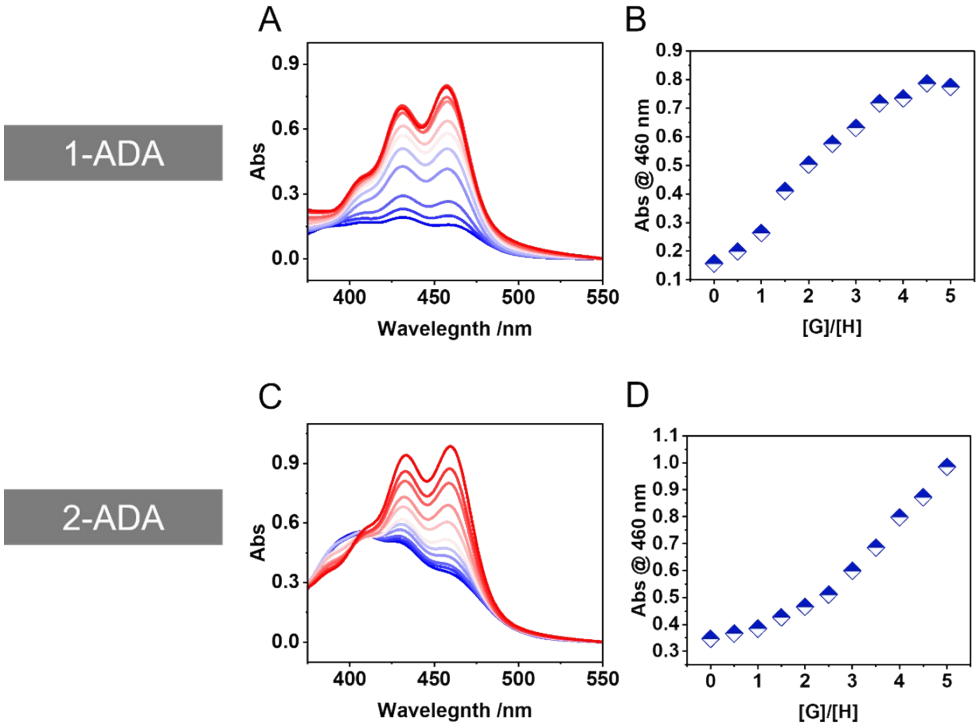

Figure S27. UV titration curves and normalized curves for the two hosts using ADA.

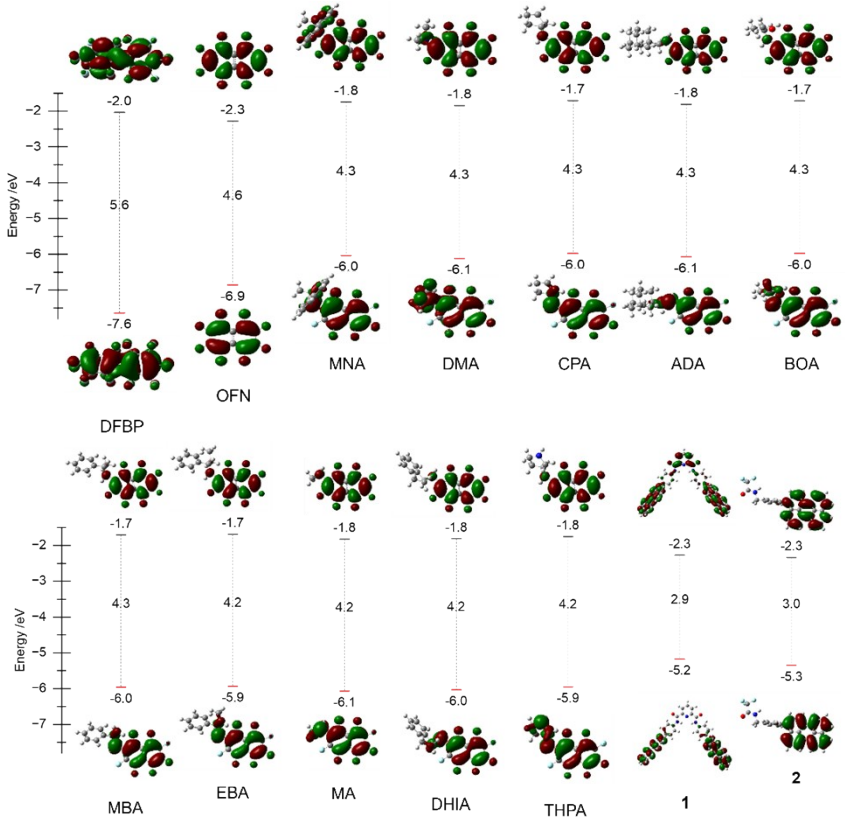

Figure S28. HOMO and LUMO, as well as energy gap of each molecule, denoted as $E_{LUMO} - E_{HOMO}$.

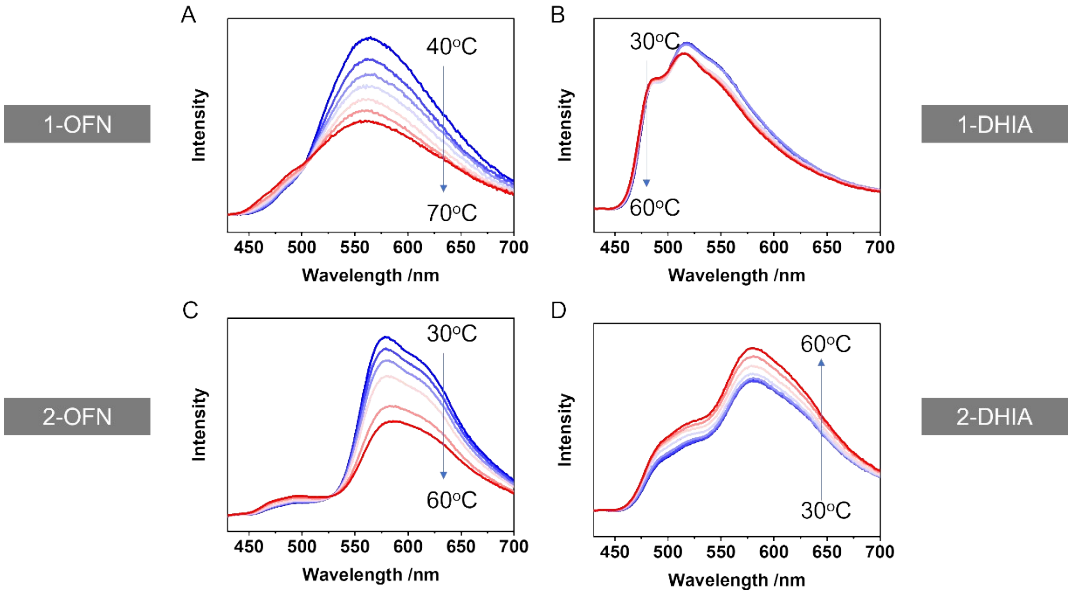

Figure S29. Temperature-dependent fluorescence. (5 e.q. guest as the host)

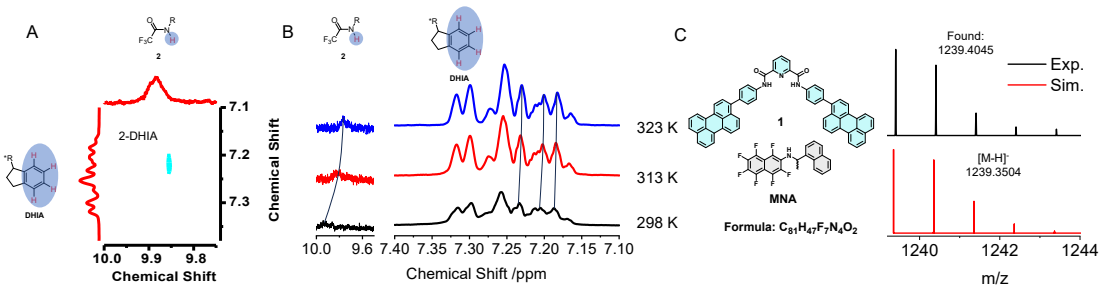

Figure S30. NOESY spectra (A) and Variable-Temperature NMR spectra (B) of DHIA with **2** (1.0 mmol·L^{-1} **2** in DMSO-d_6:$CDCl_3$ = 1:1, and 15 eq. DHIA as the **2**). C) Mass Spectra of **1**-DHIA.

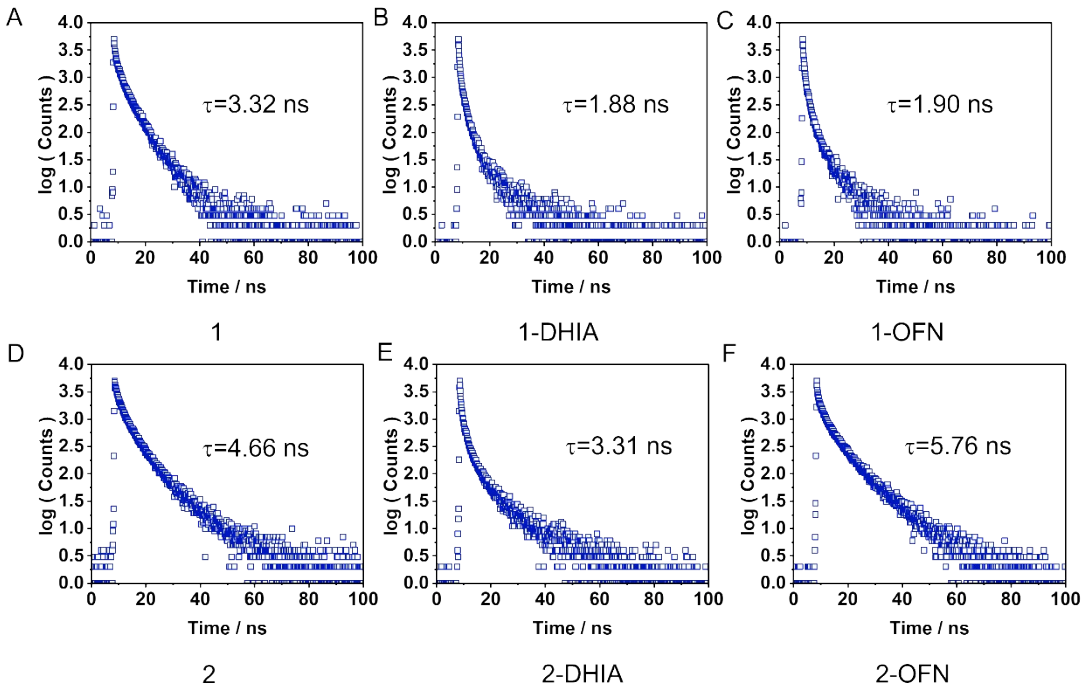

Figure S31. Fluorescence decay curve (5 e.q. guest as the host, excitation wavelength is 400 nm, and probe wavelength is 550 nm).

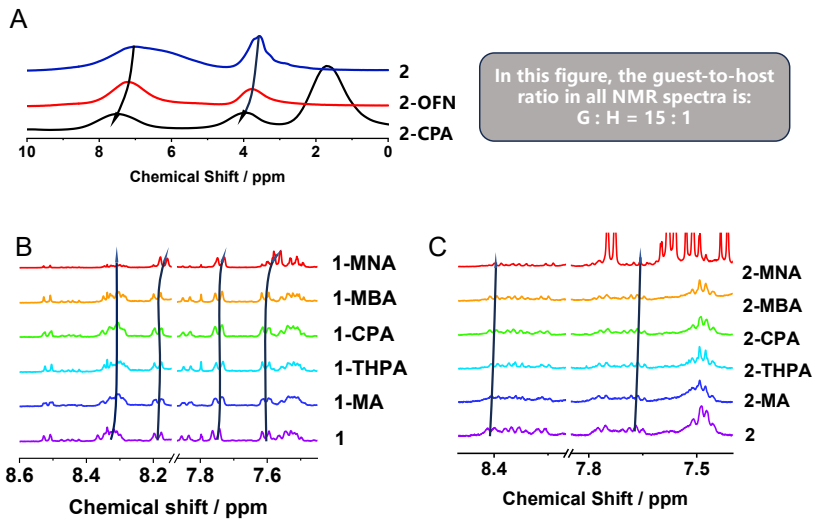

Figure S32. NMR spectra, where A presents the solid-state NMR spectra of host 2, as well as its assembled systems with OFN and CPA. Figures B and C show the NMR spectra measured in a DMSO:chloroform (1 : 1 v/v) solvent mixture, where the molar ratio of the guest to the host is 15 : 1.

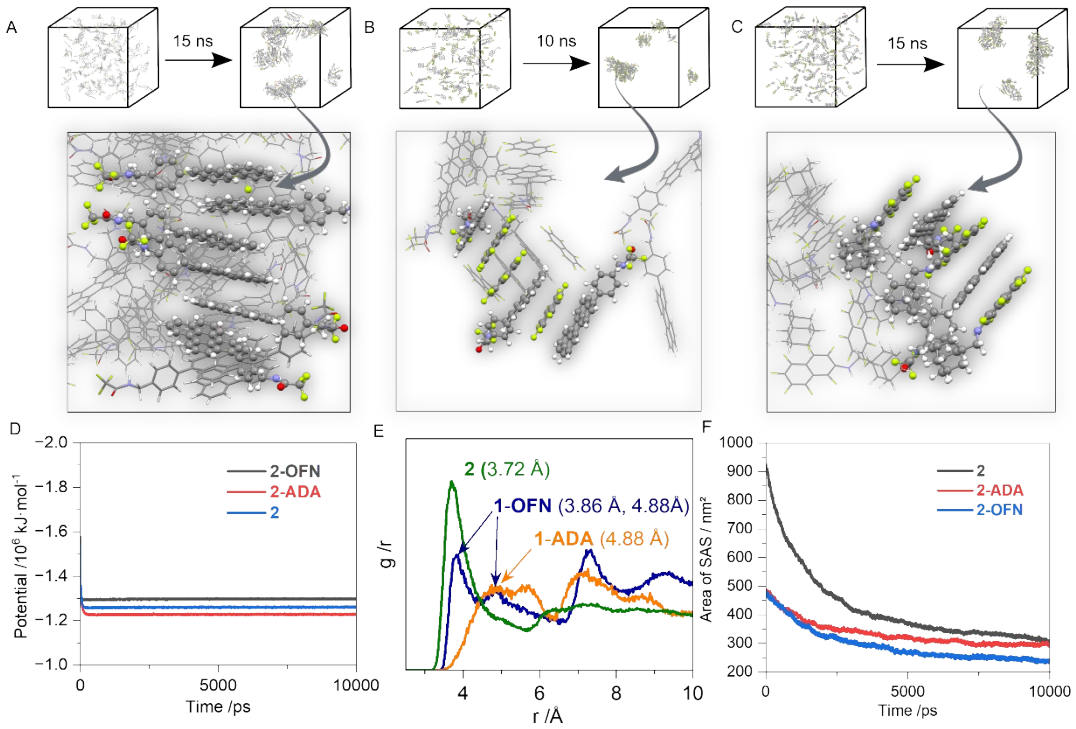

Figure S33. MD simulation. A) System of **2**. B) System of **2** and OFN. C) System of **2** and ADA. D) Potential energy of the process. E) Radial Distribution Function (RDF) profiles. F) Solvent Accessible Area.

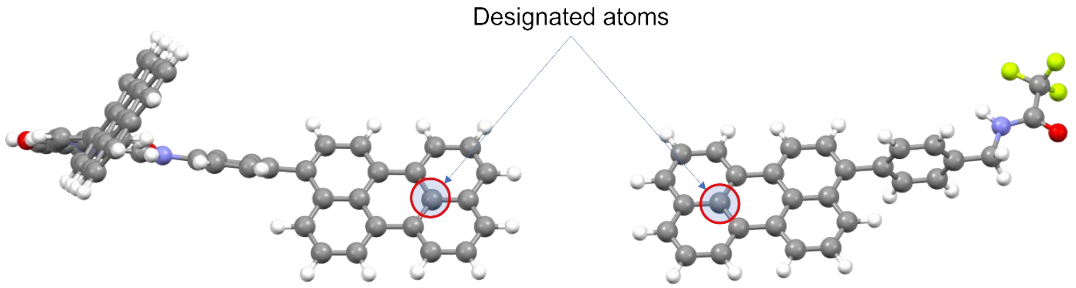

Figure S34. Designated atoms for RDF calculation.

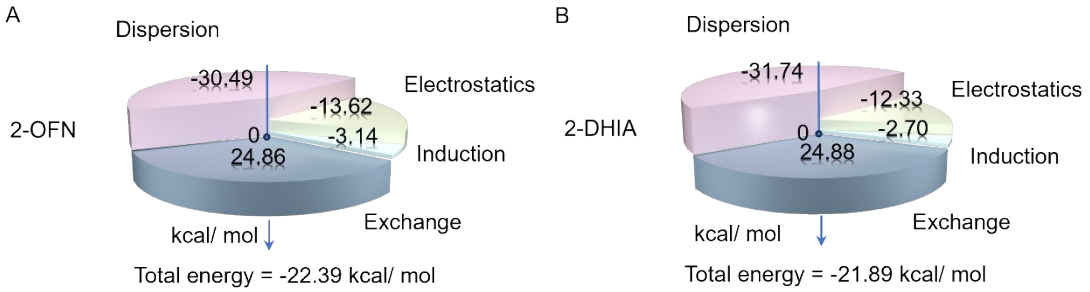

Figure S35. A) Energy decomposition of the AP interaction between **2** and OFN. B) Energy decomposition of the AP interaction between **2** and OFN.

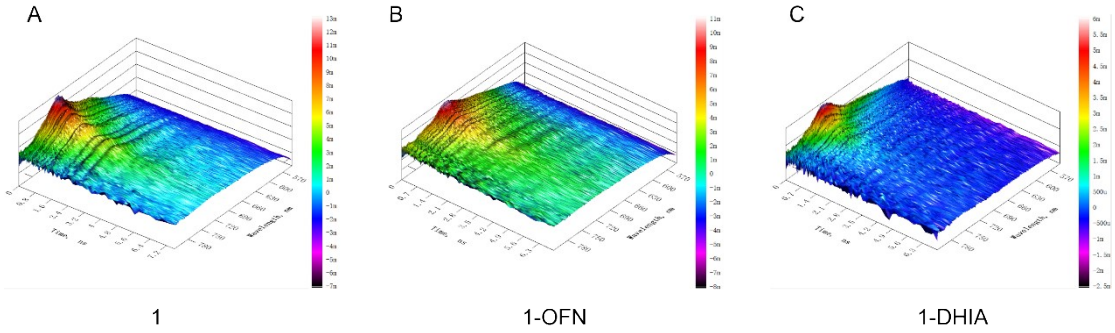

Figure S36. 3D plot of transient absorption.

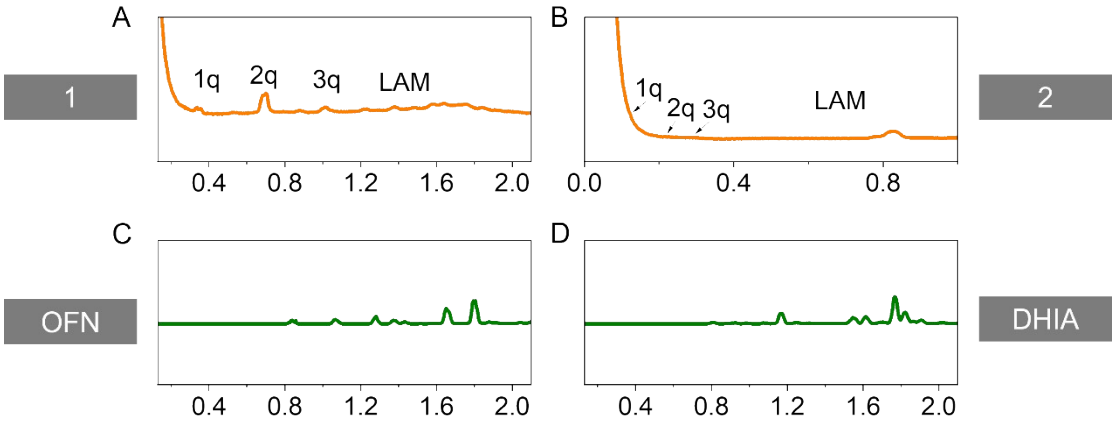

Figure S37. SAXS pattern of monomer.

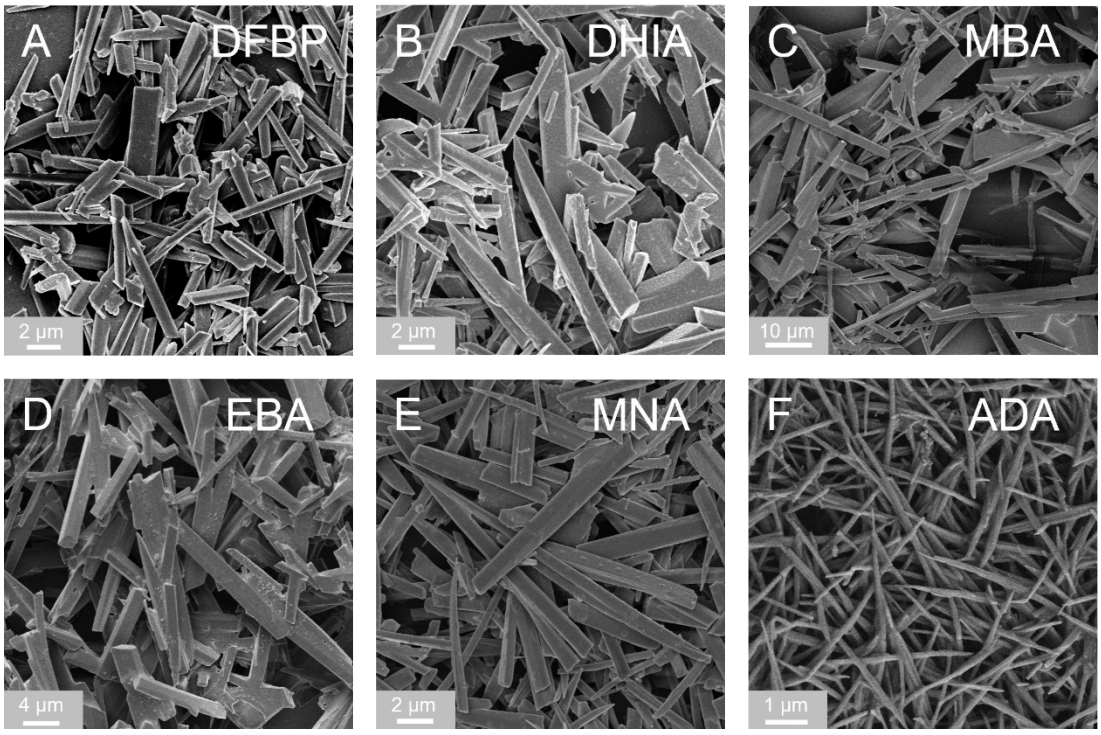

Figure S38. Morphology of the assembly after the guest molecule interacts with **1**.

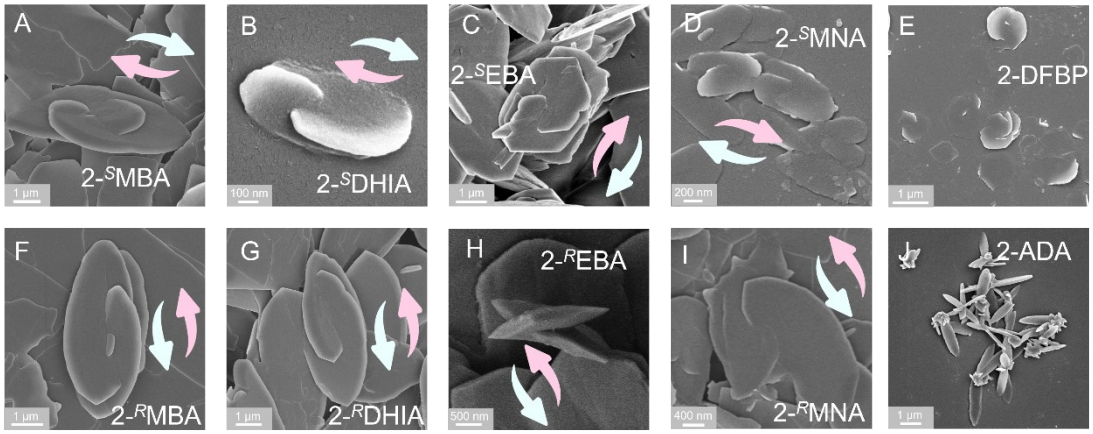

Figure S39. Morphology of the assembly after the guest molecule interacts with **2**.

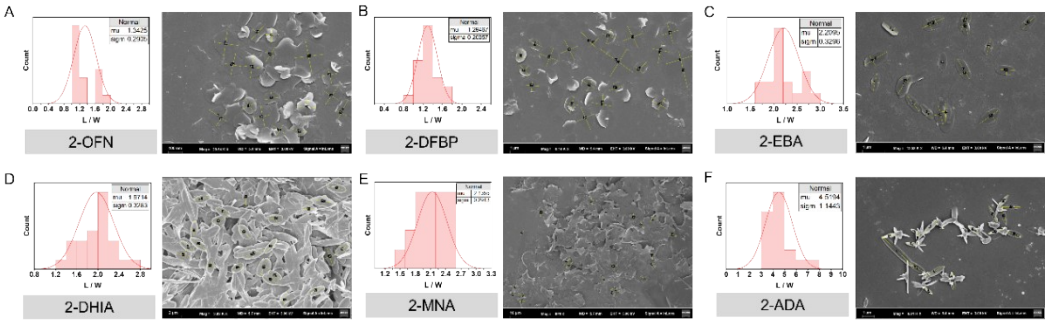

Figure S40. Aspect ratio statistics.

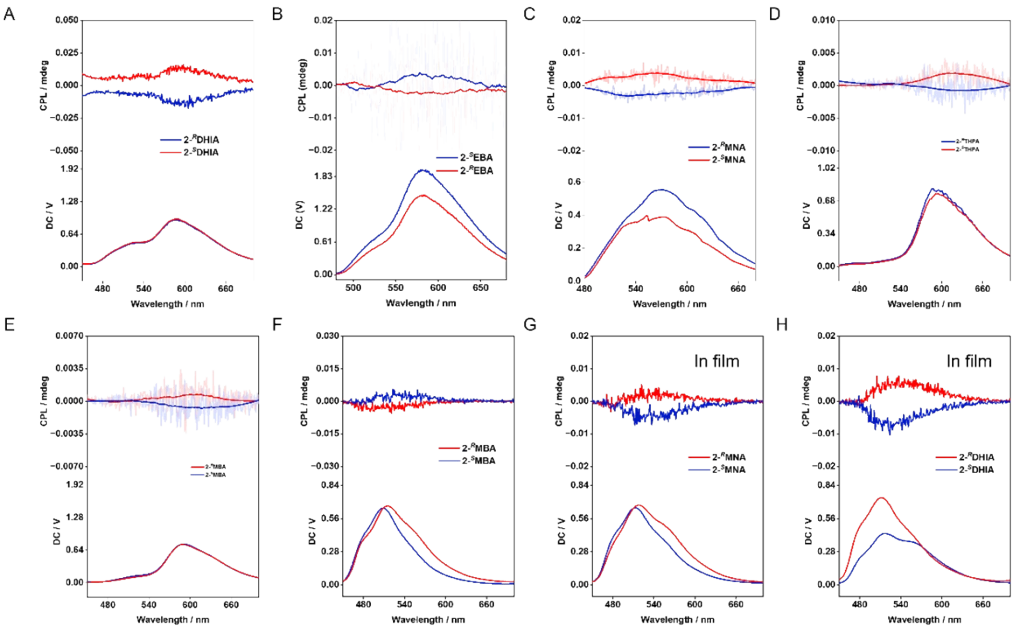

Figure S41. CPL spectra in the assembled solution and in the film.

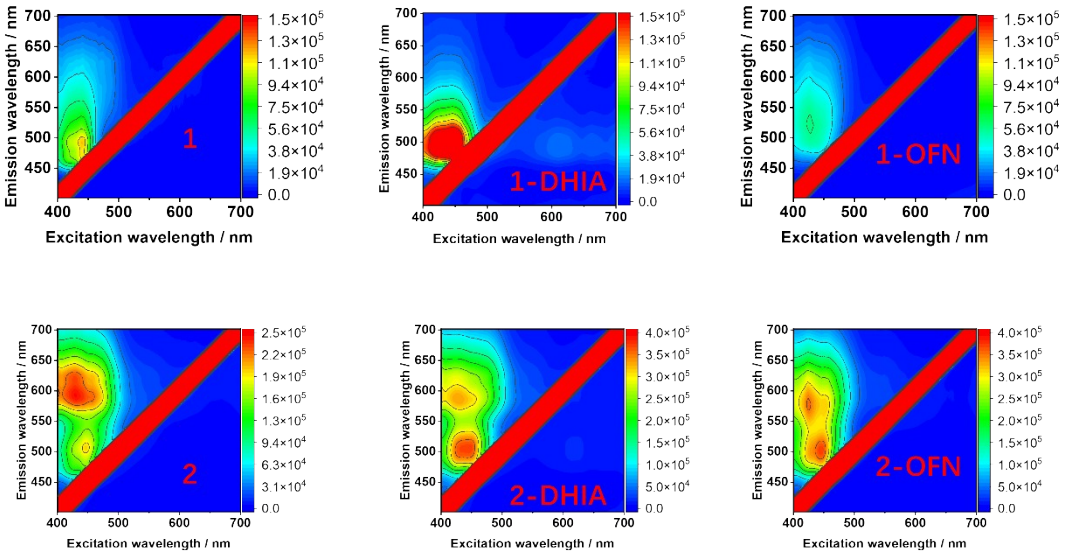

Figure S42. Two-dimensional fluorescence testing.

C.Synthesis and Characterization

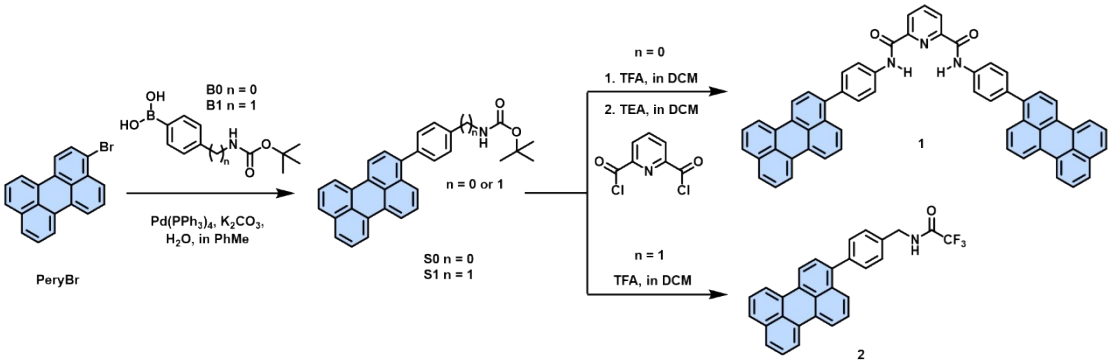

Figure S43. Synthetic route of Host.

Synthesis of S0 and S1 To obtain PeryBr according to literature methods.[S3] A solution of PeryBr (1.65 g, 5.0 mmol), B0 (1.78 g, 7.5 mmol) in toluene (150 mL) was purged with N_2 and stirred 15 min at 80 °C with N_2 bubbling. After addition of degassed aqueous potassium carbonate 2 M solution (2.5 mL, 5 mmol), of $Pd(PPh_3)_4$ (200 mg, 0.17 mmol), the mixture was stirred 24 h at 100 °C under N_2. After washing the solution three times with 100 mL of water, the organic phase was collected and dried over anhydrous $NaSO_4$. The solution was then filtered. After removing the solvent under vacuum, the product was purified by column chromatography to obtain pure S1 as a yellow powder. Yield: 1.69 g (76%). S1 was obtained from B1 using the same method, resulting in a yellow powder. Yield: 1.67 mg (73%).

Synthesis of 1 Add S0 (887 mg, 2 mmol) and 50 mL of DCM to a round-bottom flask, then drop in 1.0 mL of TFA and stir at room temperature for 2 h. Remove the solvent under vacuum, then dissolve the residue in 150 mL of DCM and add 3 mL of TEA. Subsequently, add the DCM solution of pyridine-2,6-dicarbonyl chloride (204 mg, 1 mmol) dropwise at 0 °C, then allow the mixture to return to room temperature and stir for 6 hours. The solvent was removed under vacuum, and the residue was purified by column chromatography to obtain pure **1**, which is a yellow powder. Yield: 687 mg (84%).

Synthesis of 2 Add S1 (915 mg, 2 mmol) and 50 mL of DCM to a round-bottom flask, then drop in 5.0 mL of TFA and stir at room temperature for 2 h. Then, add 5 mL of thionyl chloride and reflux for 1 h. After cooling the solution to room temperature, wash it three times with 50 mL of water, collect the organic phase, and dry it over

anhydrous sodium sulfate. The resulting solution is then purified by column chromatography to obtain pure product **2** as brown powder. Yield: 650 mg (71%).

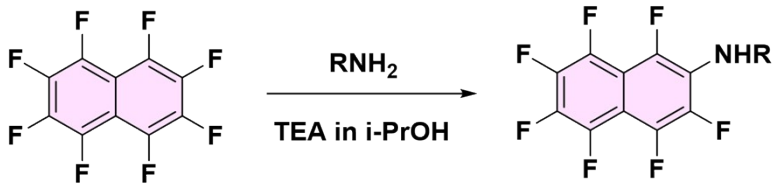

Figure S44. Synthetic route of Guest.

Synthesis of guest molecules MBA was synthesized using the method described in the literature[S3], and the other guest molecules were synthesized using the same approach.

Characterization of 1 ^{1}H NMR (500 MHz, DMSO-d_6) δ 11.26 (s, 2H), 8.52 – 8.36 (m, 12H), 8.19 – 8.15 (m, 4H), 7.81 (dd, J = 11.7, 8.3 Hz, 6H), 7.65 (d, J = 8.5 Hz, 4H), 7.61 – 7.51 (m, 8H). ^{13}C NMR (101 MHz, DMSO-d_6) δ 161.19, 148.28, 138.39, 135.22, 133.71, 131.69, 130.28, 129.99, 129.82, 129.54, 129.31, 128.19, 127.80, 127.36, 127.22, 126.53, 126.39, 120.43, 120.36, 120.11, 119.93. HRMS m/z $[M+H]^+$, calculated for $C_{59}H_{36}N_3O_2$, 818.2802; found 818.2802.

Characterization of 2 ^{1}H NMR (400 MHz, DMSO-d_6) δ 10.13 (t, J = 6.1 Hz, 1H), 8.41 (dd, J = 10.5, 7.8 Hz, 4H), 7.82 (d, J = 8.1 Hz, 2H), 7.68 (d, J = 8.4 Hz, 1H), 7.59 – 7.50 (m, 5H), 7.49 – 7.43 (m, 3H), 4.52 (d, J = 6.0 Hz, 2H). ^{13}C NMR (101 MHz, DMSO-d_6) δ 192.24, 139.03 – 116.21 (m), 129.19. HRMS m/z $[M]^+$, calculated for $C_{29}H_{18}F_3NO$, 453.1335; found 453.1339.

Characterization of THPA ^{1}H NMR (400 MHz, Chloroform-*d*) δ 3.06 (ddt, J = 10.6, 4.7, 3.0 Hz, 2H), 3.01 – 2.89 (m, 1H), 2.79 (p, J = 5.9 Hz, 1H), 2.65 (ddt, J = 8.4, 5.7, 3.1 Hz, 1H), 1.37 (ddt, J = 12.0, 7.6, 5.9 Hz, 1H), 1.00 (ddd, J = 13.9, 12.4, 6.7 Hz, 1H). ^{19}F NMR (376 MHz, Chloroform-*d*) δ -136.42 (dt, J = 72.0, 12.8 Hz), -141.46 – -141.64 (m), -146.27 – -146.92 (m), -148.13 (dt, J = 55.1, 13.4 Hz), -156.53 (ddd, J = 19.3, 14.0, 7.9 Hz), -160.51 (td, J = 19.5, 18.8, 4.1 Hz). HRMS m/z $[M+H]^+$, calculated for $C_{14}H_{10}F_7N_2$, 339.0727; found 339.0724.

Characterization of BOA ^{1}H NMR (400 MHz, DMSO-d_6) δ 5.58 (s, 1H), 1.69 – 1.46 (m, 2H), 1.41 – 1.31 (m, 1H), 1.31 – 1.16 (m, 2H), 0.93 (t, J = 7.4 Hz, 3H). ^{19}F

NMR (376 MHz, Chloroform-*d*) δ -142.85 (t, *J* = 11.3 Hz), -142.94 – -143.11 (m), -147.32 (dtd, *J* = 56.0, 17.3, 16.4, 5.3 Hz), -148.18 (dt, *J* = 63.2, 15.9 Hz), -148.78 – -149.30 (m), -156.49 (td, *J* = 19.3, 5.9 Hz), -160.06 (t, *J* = 18.6 Hz). HRMS m/z $[M+H]^+$, calculated for $C_{14}H_{11}F_7NO$, 342.0723; found 342.0739.

Characterization of EBA ^{1}H NMR (400 MHz, DMSO-d_6) δ 7.37 (d, *J* = 7.6 Hz, 2H), 7.29 (t, *J* = 7.5 Hz, 2H), 7.18 (t, *J* = 7.2 Hz, 1H), 6.47 (d, *J* = 9.3 Hz, 1H), 4.72 – 4.62 (m, 1H), 2.00 (dq, *J* = 14.9, 7.5 Hz, 1H), 1.77 (dp, *J* = 14.1, 7.2 Hz, 1H), 1.39 – 1.21 (m, 1H), 0.94 (t, *J* = 7.3 Hz, 3H).^{13}C NMR (101 MHz, DMSO-d_6) δ 144.77, 128.81, 127.41, 126.63, 61.67, 31.13, 12.01. HRMS m/z $[M+H]^+$, calculated for $C_{19}H_{13}F_7N$, 338.0931; found 338.0936.

Characterization of MNA ^{1}H NMR (400 MHz, DMSO-d_6) δ 8.22 (d, *J* = 8.4 Hz, 1H), 7.93 (dd, *J* = 8.1, 1.6 Hz, 1H), 7.77 (d, *J* = 8.2 Hz, 1H), 7.64 – 7.49 (m, 3H), 7.44 (dd, *J* = 8.1, 7.2 Hz, 1H), 6.81 (dt, *J* = 8.4, 2.7 Hz, 1H), 5.90 (q, *J* = 7.2 Hz, 1H), 1.65 (d, *J* = 6.7 Hz, 3H).^{19}F NMR (377 MHz, DMSO-d_6) δ -143.09 (t, *J* = 12.4 Hz), -143.26 (t, *J* = 12.5 Hz), -146.79 (ddt, *J* = 17.2, 11.6, 5.9 Hz), -148.65 (dddd, *J* = 54.7, 19.0, 14.0, 4.3 Hz), -149.49 (dddd, *J* = 64.5, 18.6, 14.2, 3.3 Hz), -150.43 – -150.75 (m), -157.34 – -157.59 (m), -161.96 – -162.19 (m). HRMS m/z $[M+H]^+$, calculated for $C_{22}H_{13}F_7N$, 424.0931; found 424.0935.

Characterization of DHIA ^{1}H NMR (400 MHz, DMSO-d_6) δ 7.32 – 7.14 (m, 4H), 6.38 (dt, *J* = 9.3, 2.6 Hz, 1H), 5.34 (q, *J* = 8.1 Hz, 1H), 3.00 (ddd, *J* = 15.9, 8.8, 3.3 Hz, 1H), 2.83 (dt, *J* = 16.0, 8.3 Hz, 1H), 2.09 (dq, *J* = 12.7, 8.4 Hz, 1H). ^{13}C NMR (101 MHz, DMSO-d_6) δ 145.00, 143.33, 128.09, 126.92, 125.10, 124.33, 60.62, 34.60, 29.98. HRMS m/z $[M-H]^-$, calculated for $C_{19}H_9F_7N$, 384.0618; found 384.0609.

Characterization of MA ^{1}H NMR (400 MHz, Chloroform-*d*) δ 3.21 (dd, *J* = 3.3, 2.1 Hz, 3H). ^{19}F NMR (376 MHz, Chloroform-*d*) δ -145.73 (dt, *J* = 64.2, 13.5 Hz), -147.56 (dt, *J* = 56.2, 16.4 Hz), -148.70 (dt, *J* = 63.8, 16.1 Hz), -149.71 (dt, *J* = 56.2, 15.4 Hz), -150.52 – -150.72 (m), -156.72 – -156.96 (m), -160.93, -160.93 (d, *J* = 37.7 Hz). HRMS m/z $[M+H]^+$, calculated for $C_{11}H_5F_7N$, 284.0305; found 284.0303.

Characterization of DMA ^{1}H NMR (400 MHz, Chloroform-*d*) δ 1.67 (s, 1H).^{19}F NMR (376 MHz, Chloroform-*d*) δ -133.48 (dd, *J* = 15.0, 7.0 Hz), -133.67 (dd, *J* = 14.0, 7.1 Hz), -142.00 – -142.19 (m), -146.53 (dt, *J* = 68.9, 16.3 Hz), -147.25 (dtd, *J* = 56.9, 16.9, 4.8 Hz), -148.93 (dt, *J* = 57.0, 16.2 Hz), -156.63 (td, *J* = 21.0, 19.3, 9.1 Hz), -158.08 (t, *J* = 18.9 Hz). HRMS m/z $[M+H]^+$, calculated for $C_{12}H_7F_7N$, 298.0461; found 298.0427.

Characterization of CPA ^{1}H NMR (400 MHz, Chloroform-*d*) δ 4.29 (ddq, *J* = 9.2, 6.4, 2.8 Hz, 1H), 2.12 – 1.96 (m, 2H), 1.82 – 1.60 (m, 4H), 1.52 (dq, *J* = 12.9, 6.0 Hz, 2H), 1.32 – 1.22 (m, 1H). ^{19}F NMR (377 MHz, Chloroform-*d*) δ -144.40 (td, *J* = 10.5, 9.9, 4.8 Hz), -144.51 – -144.64 (m), -147.44 – -147.75 (m), -148.45 – -148.61 (m), -148.62 – -148.78 (m), -149.51 (ddd, *J* = 18.7, 10.4, 4.1 Hz), -149.61 – -149.77 (m), -156.81 – -157.00 (m), -160.88 – -161.06 (m). HRMS m/z $[M+H]^+$, calculated for $C_{15}H_{11}F_7N$, 298.0461; found 298.0427.

Characterization of ADA ^{1}H NMR (400 MHz, Chloroform-*d*) δ 3.19 (t, *J* = 1.5 Hz, 2H), 2.01 (s, 3H), 1.79 – 1.62 (m, 12H). ^{19}F NMR (376 MHz, Chloroform-*d*) δ -137.88 (dd, *J* = 14.9, 5.3 Hz), -138.05 (dd, *J* = 14.4, 5.4 Hz), -145.59 (td, *J* = 16.8, 3.7 Hz), -145.68 – -145.84 (m), -146.24 – -146.41 (m), -146.49 (t, *J* = 16.6 Hz), -147.32 – -147.61 (m), -155.78 (tdd, *J* = 22.3, 7.4, 4.2 Hz), -155.94 – -156.13 (m). HRMS m/z $[M+H]^+$, calculated for $C_{21}H_{19}F_7N$, 418.1400; found 418.1399.

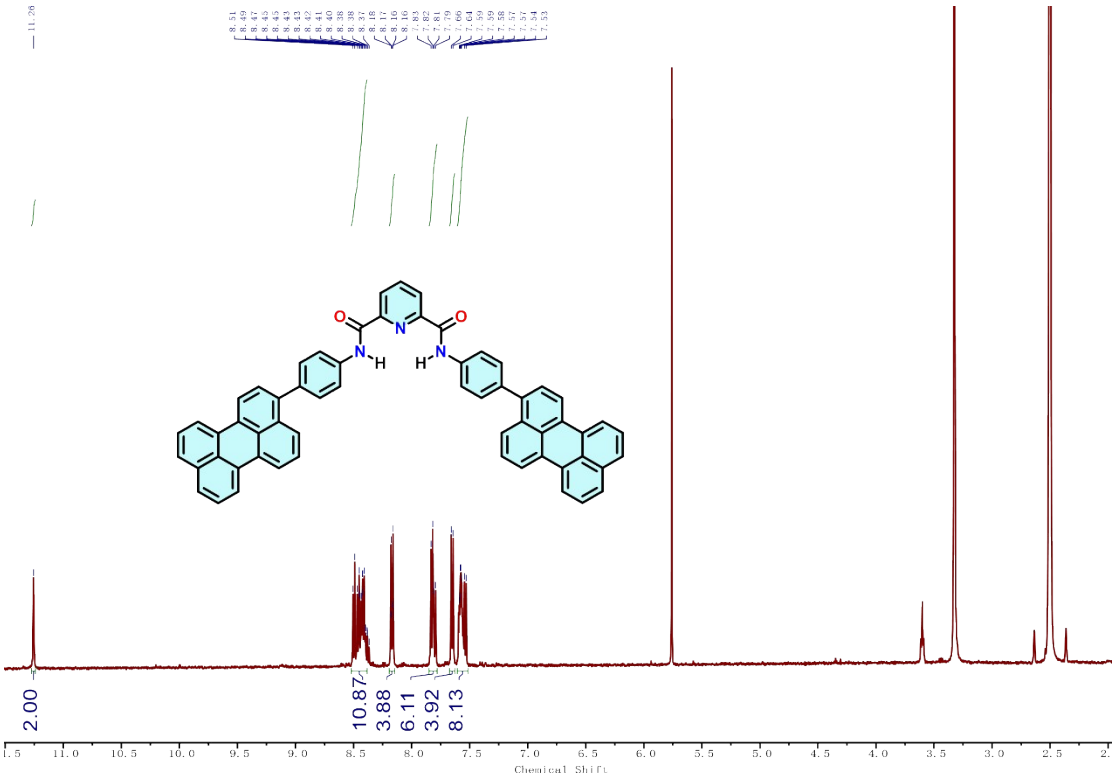

Figure S45. ^{1}H NMR spectra of **1**.

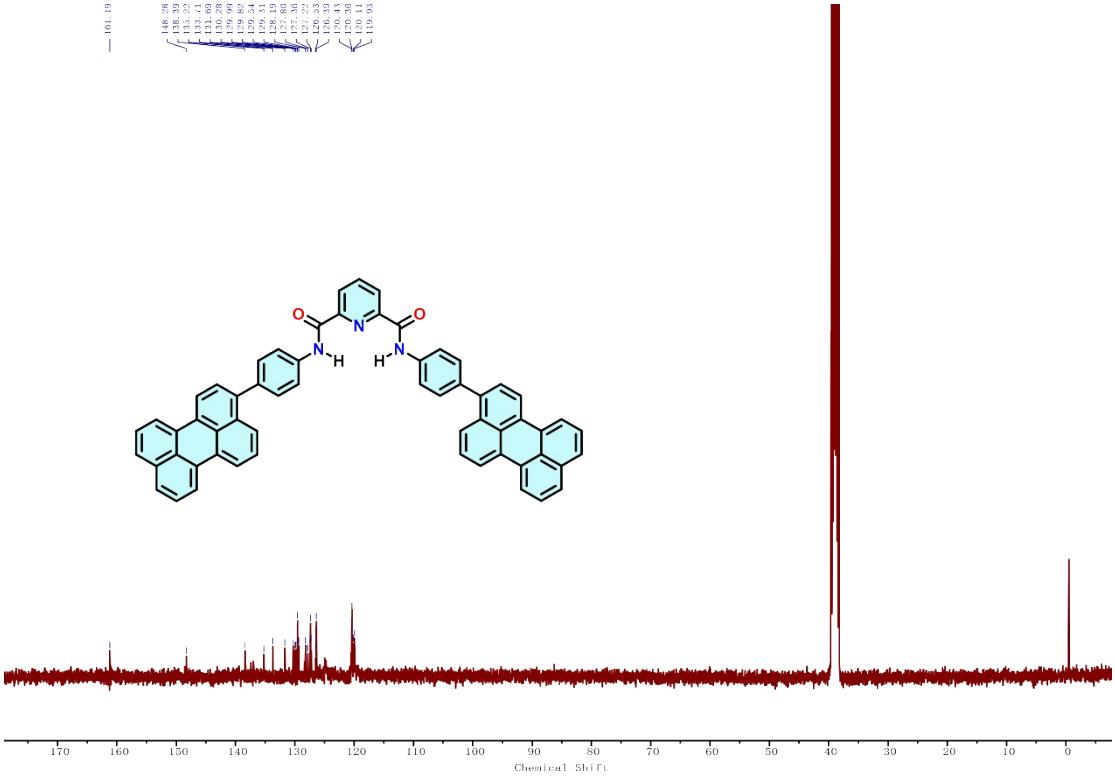

Figure S46. ^{13}C NMR spectra of **1**.

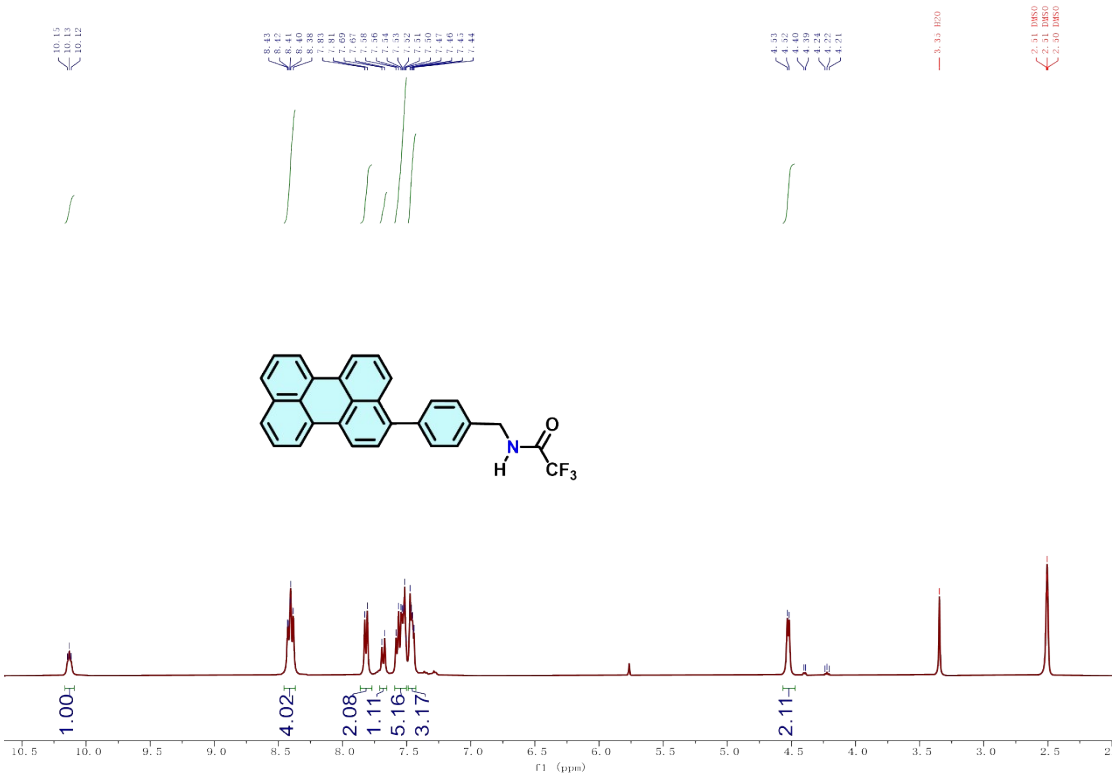

Figure S47. ^{1}H NMR spectra of **2**.

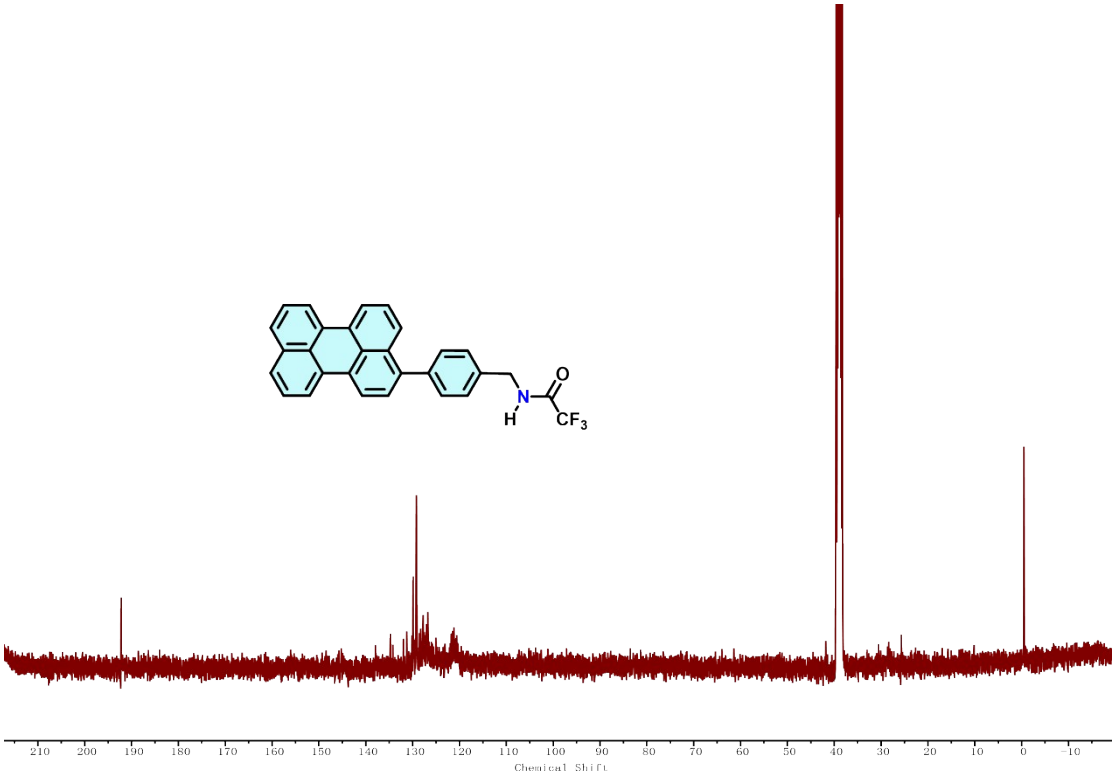

Figure S48. ^{13}C NMR spectra of **2**.

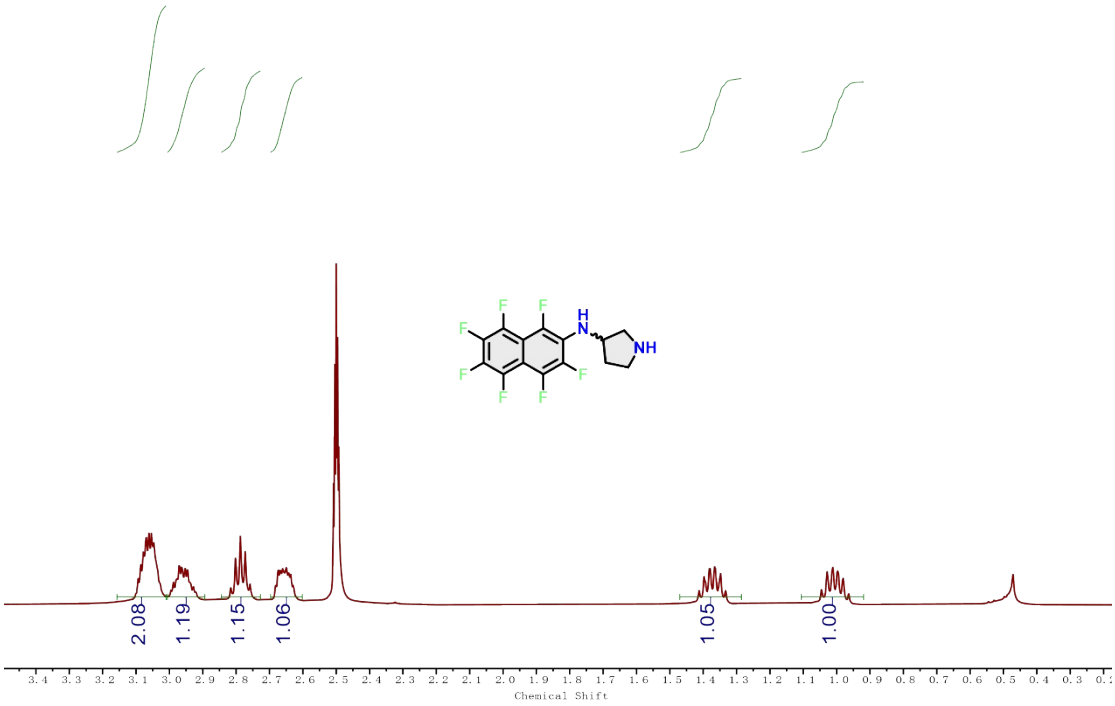

Figure S49. ^{1}H NMR spectra of THPA.

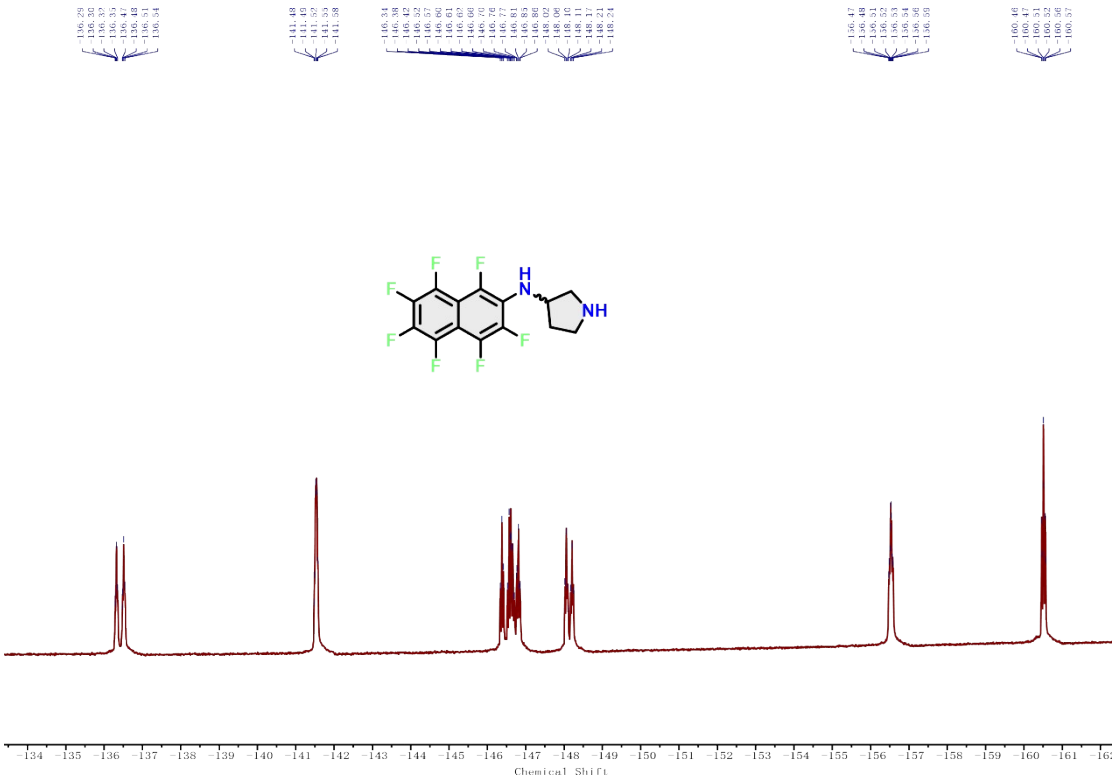

Figure S50. ^{19}F NMR spectra of THPA.

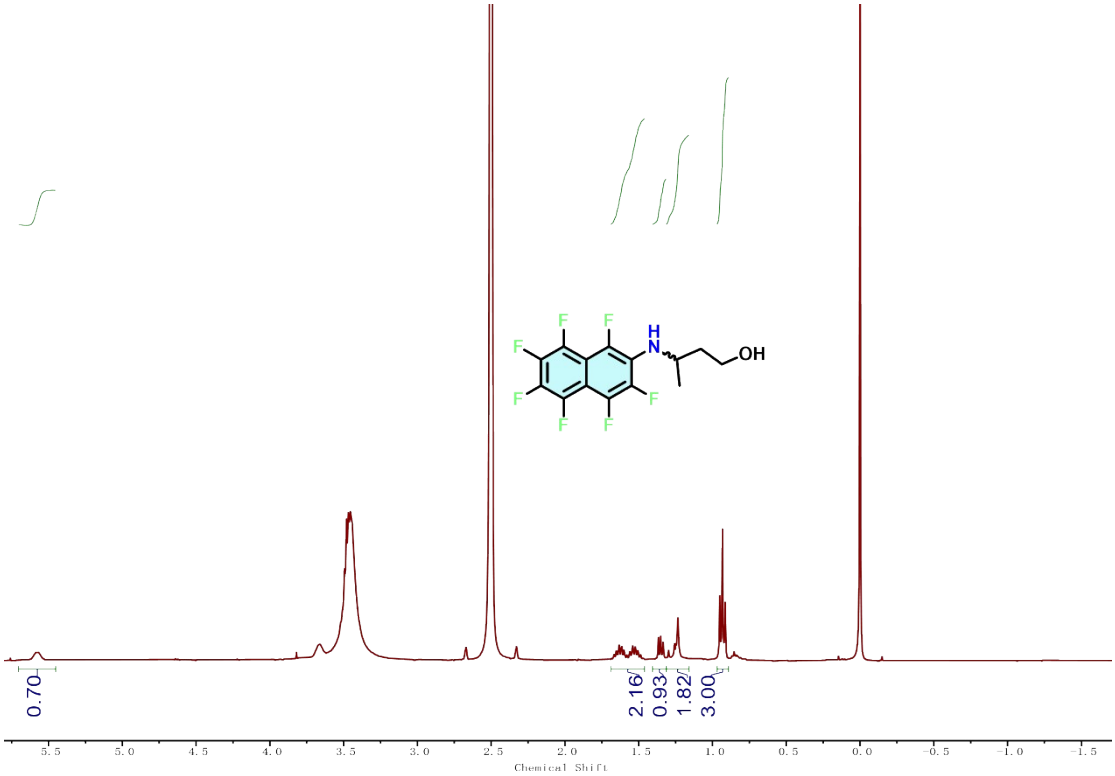

Figure S51. ^{1}H NMR spectra of BOA.

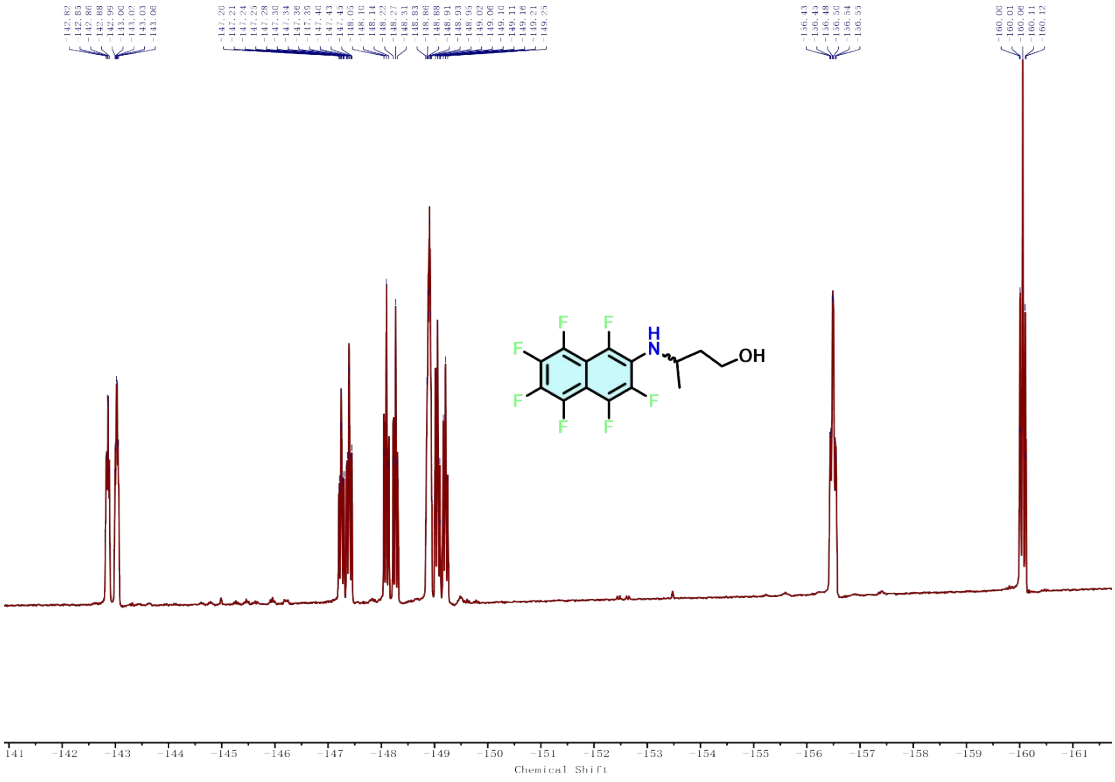

Figure S52. ^{19}F NMR spectra of BOA.

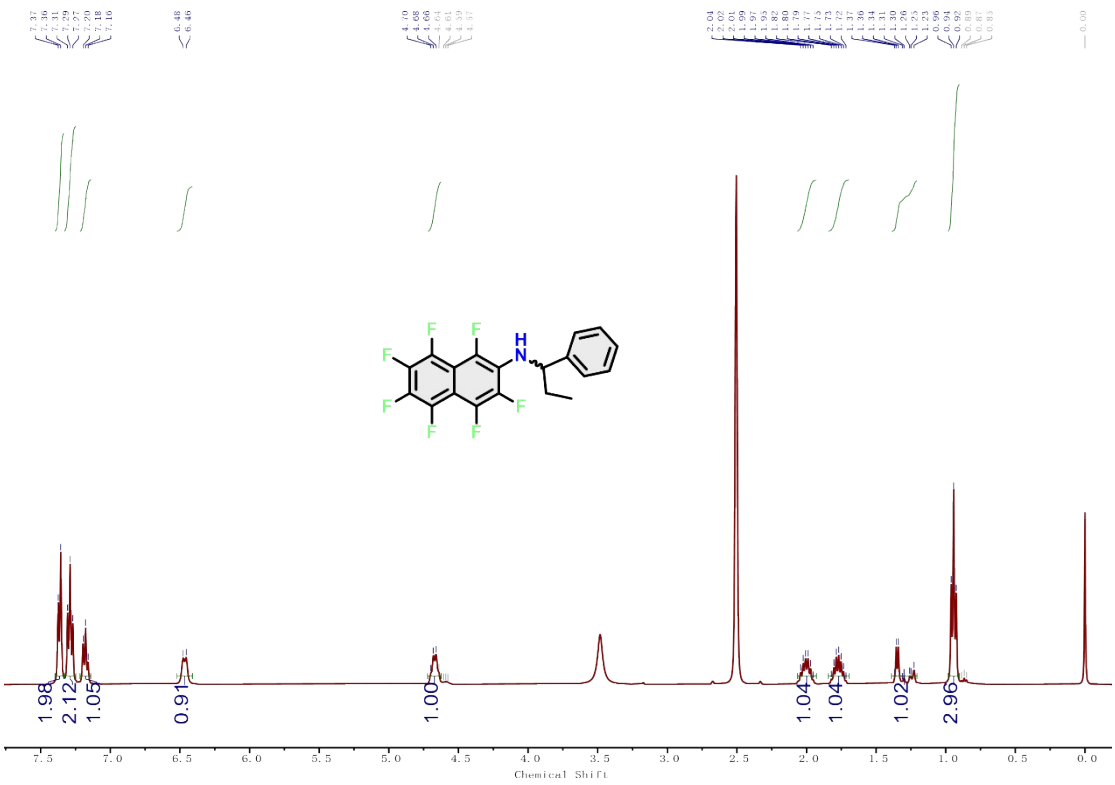

Figure S53. ^{1}H NMR spectra of EBA.

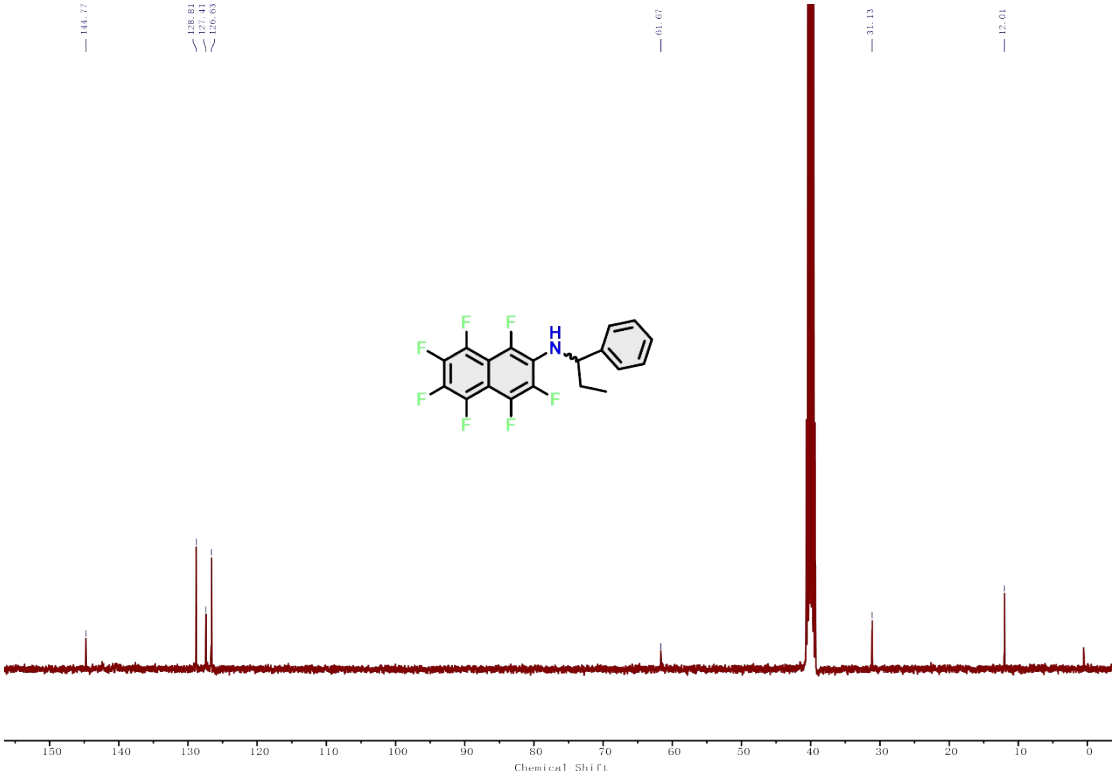

Figure S54. ^{13}C NMR spectra of EBA.

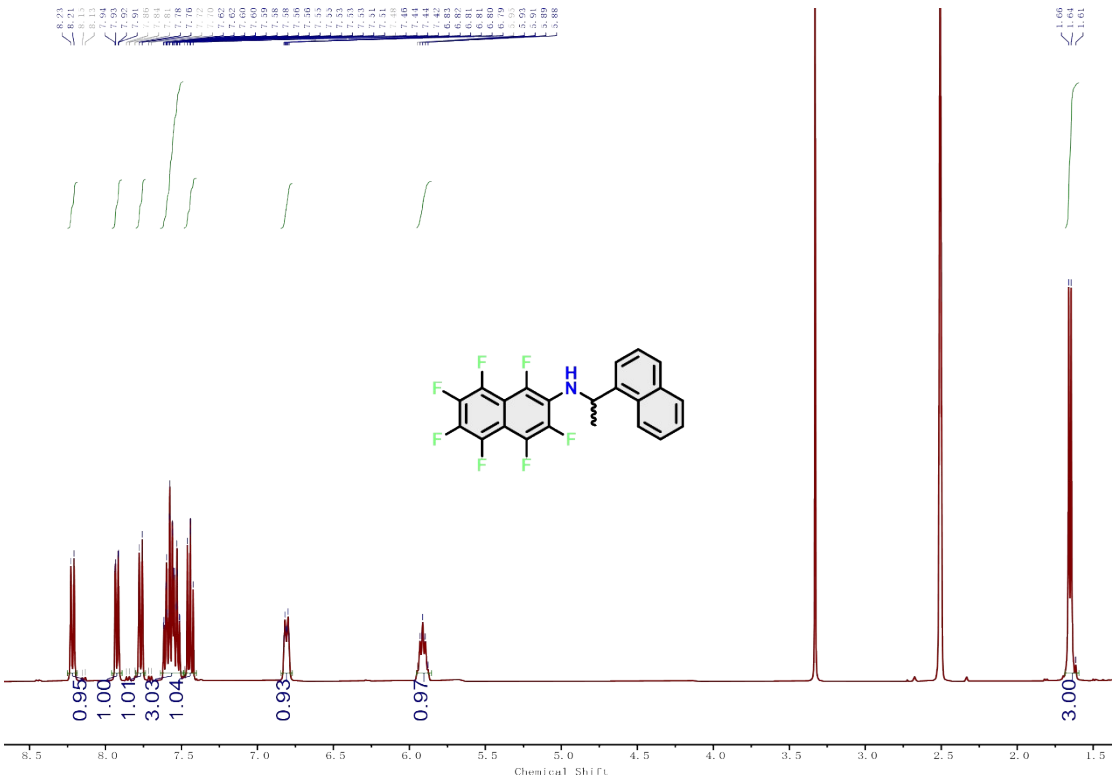

Figure S55. ^{1}H NMR spectra of MNA.

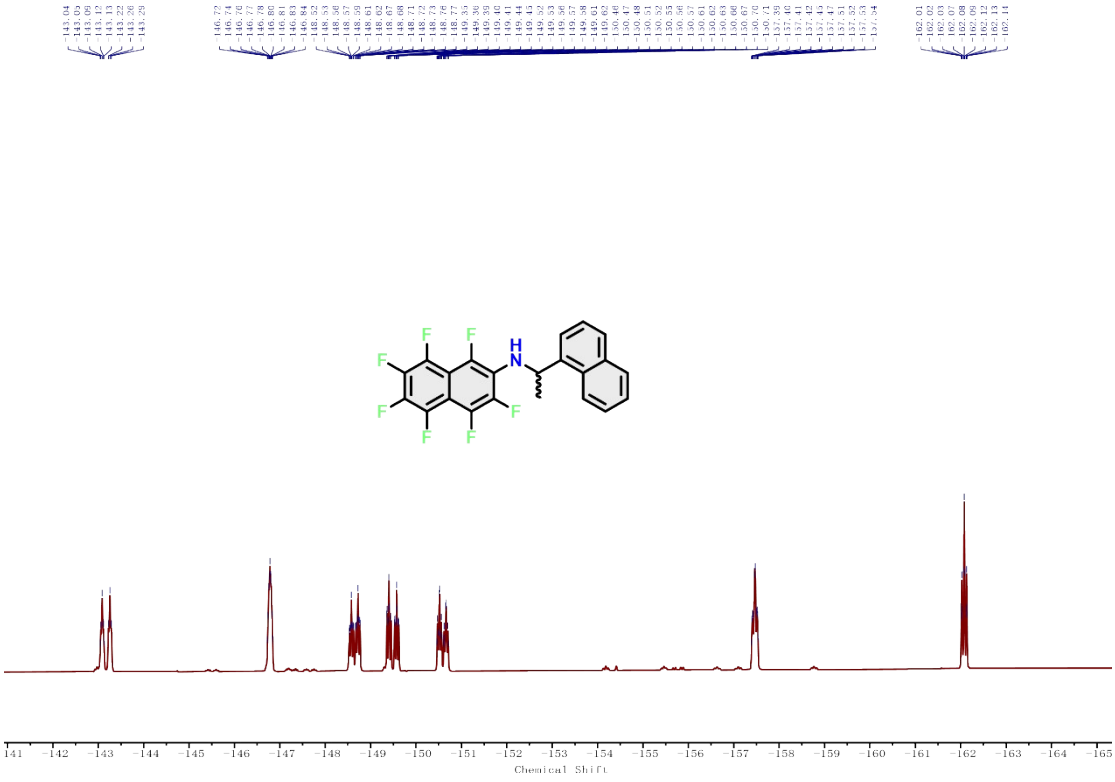

Figure S56. ^{19}F NMR spectra of MNA.

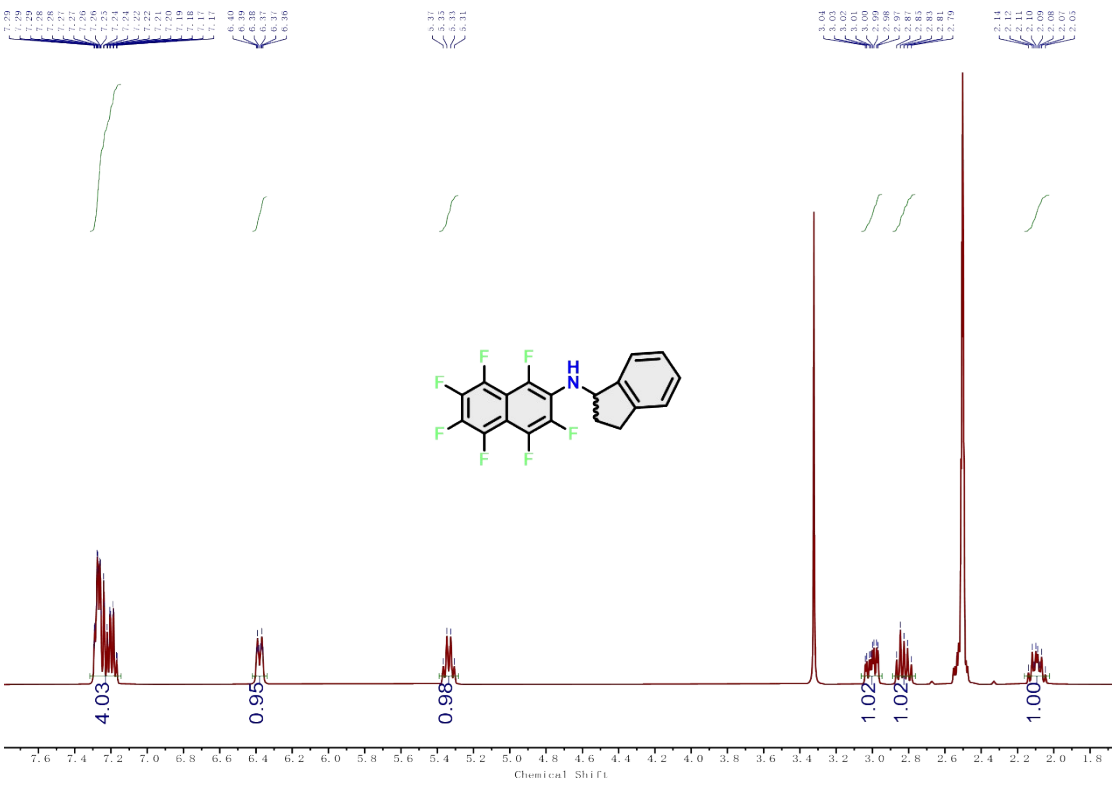

Figure S57. ^{1}H NMR spectra of DHIA.

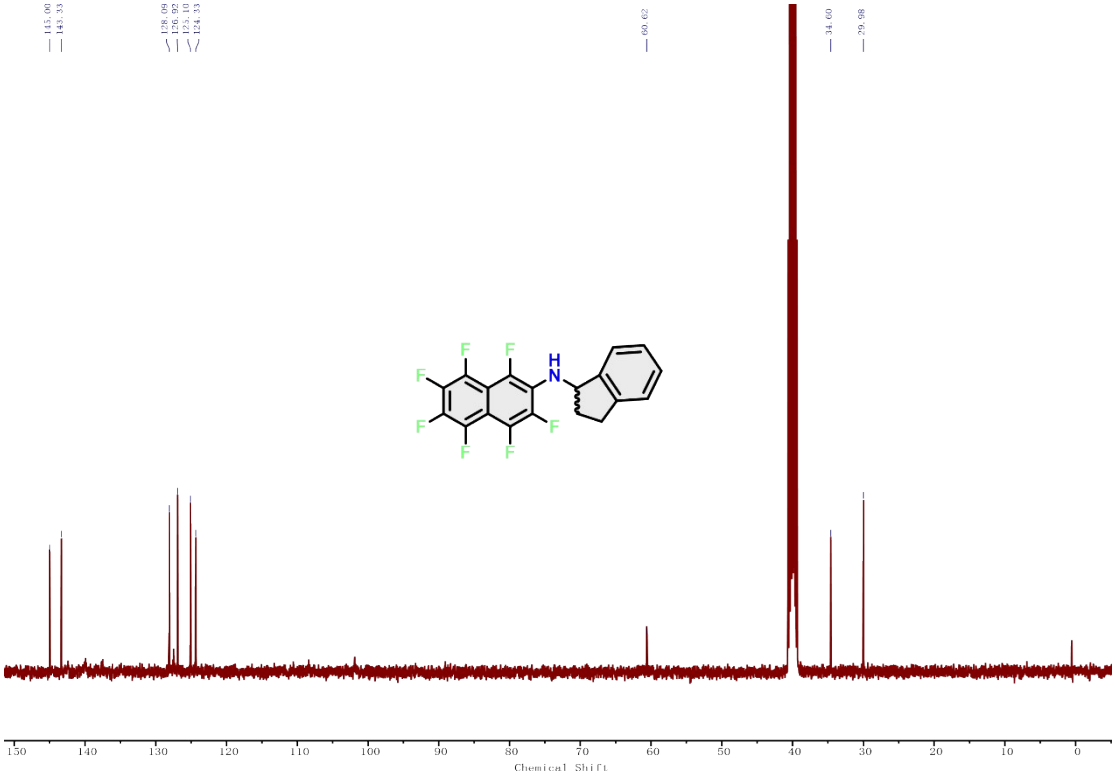

Figure S58. ^{13}C NMR spectra of DHIA.

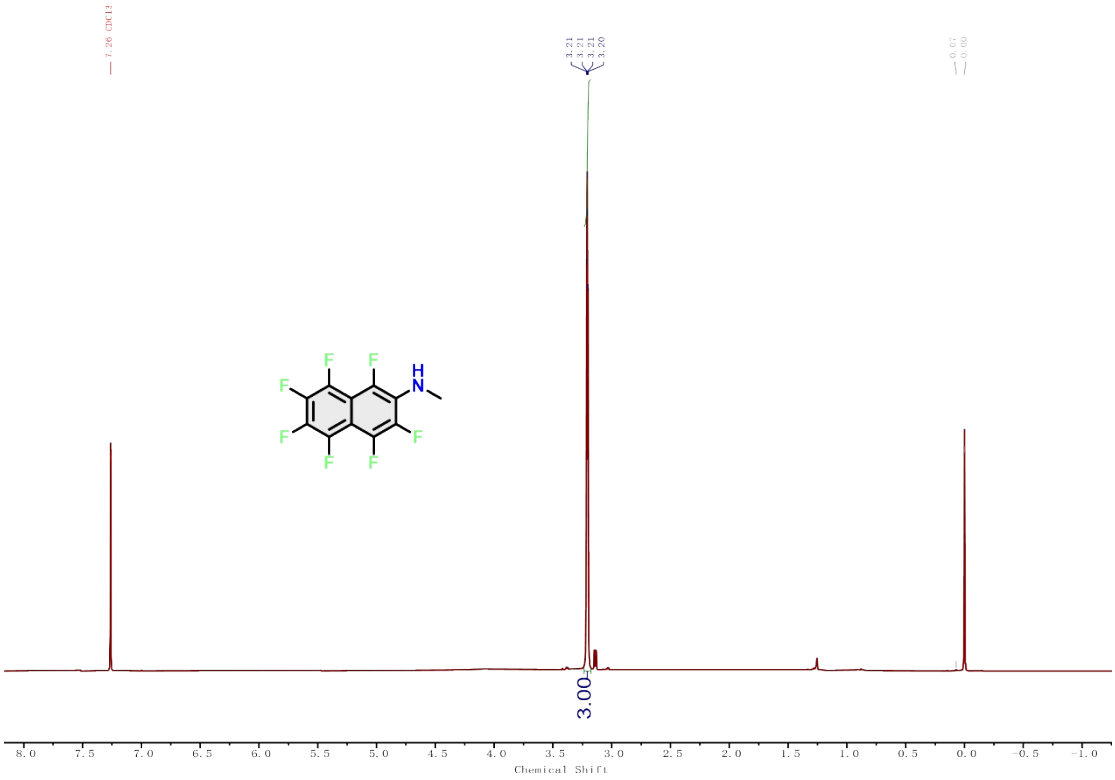

Figure S59. ^{1}H NMR spectra of MA.

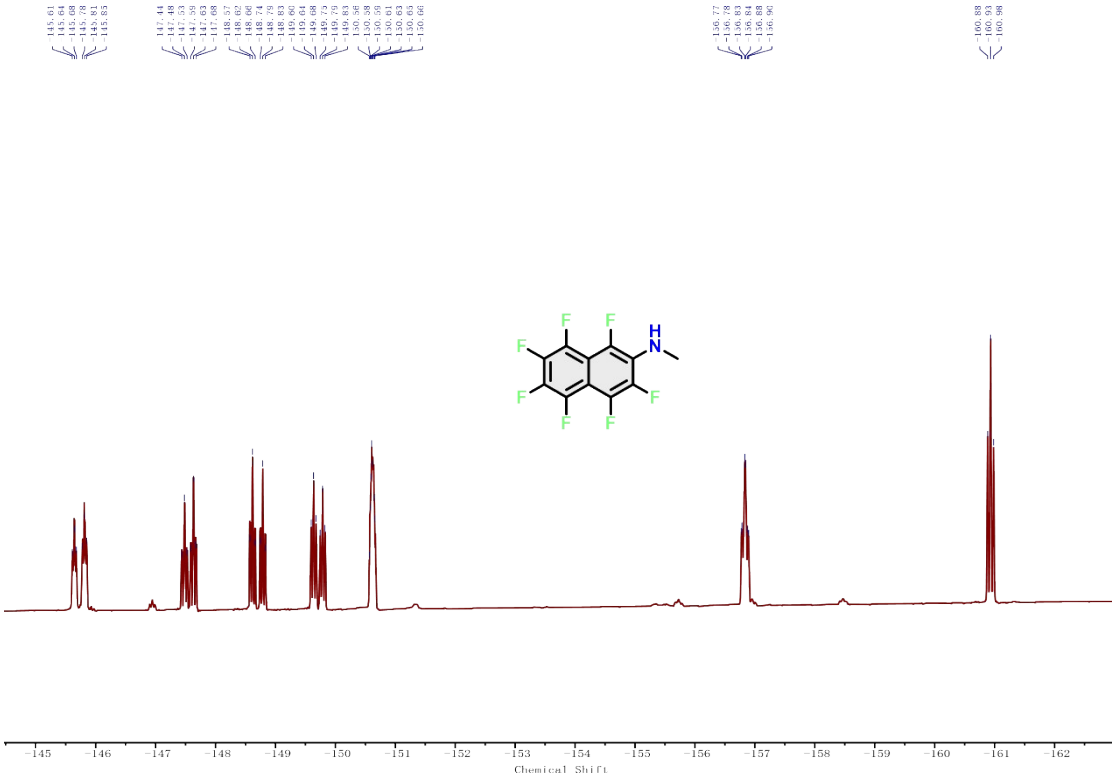

Figure S60. ^{19}F NMR spectra of MA.

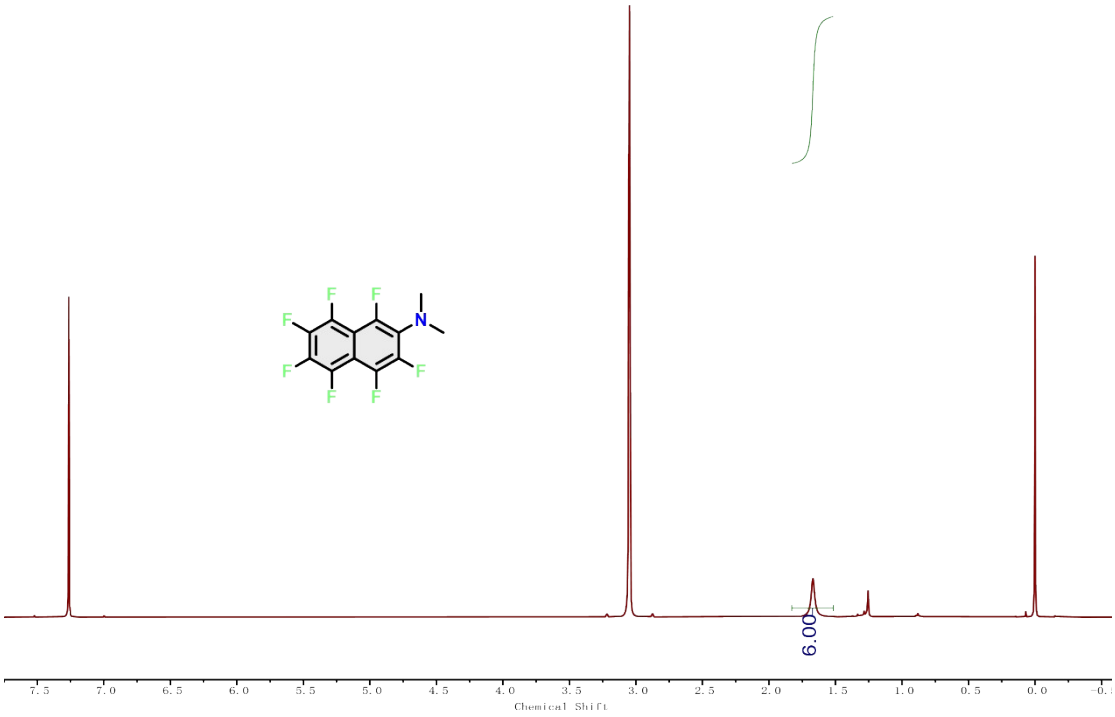

Figure S61. ^{1}H NMR spectra of DMA.

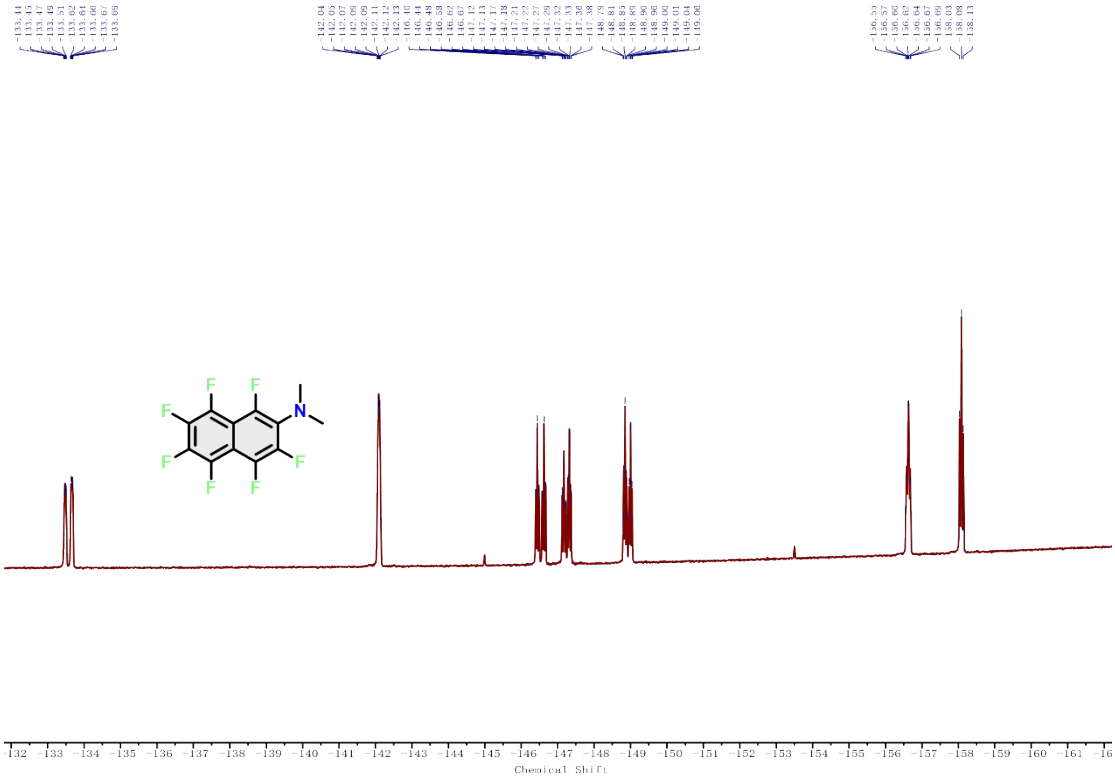

Figure S62. ^{19}F NMR spectra of DMA.

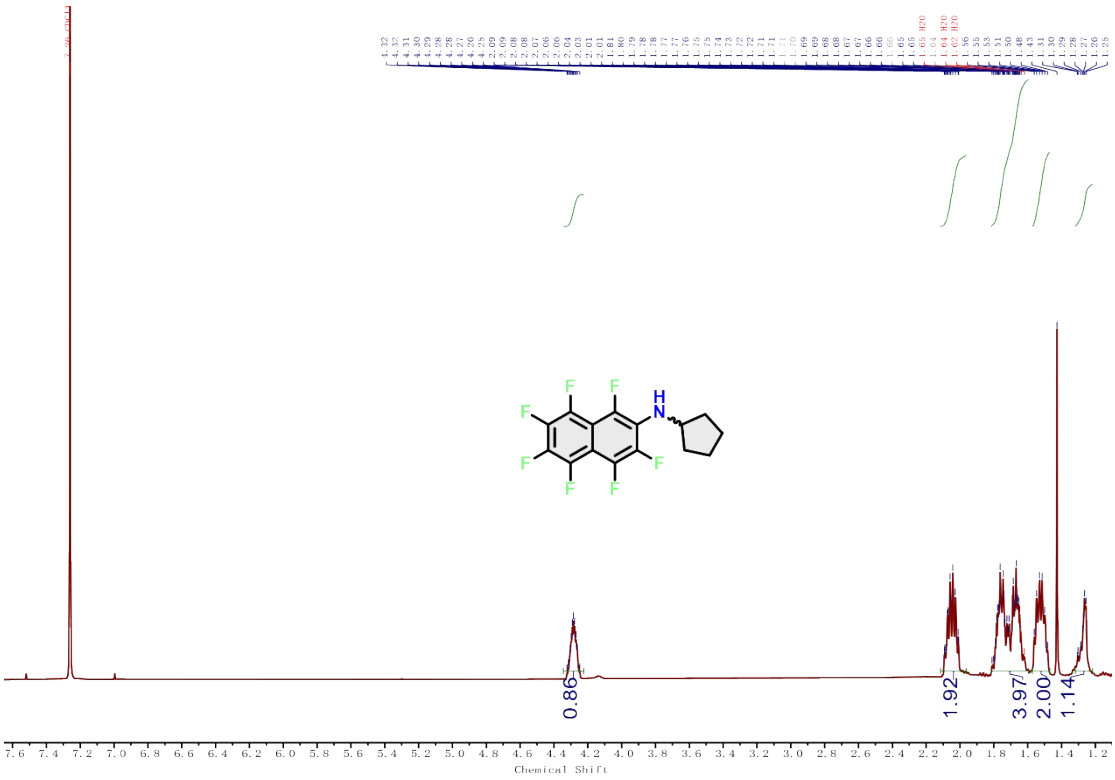

Figure S63. ^{1}H NMR spectra of CPA.

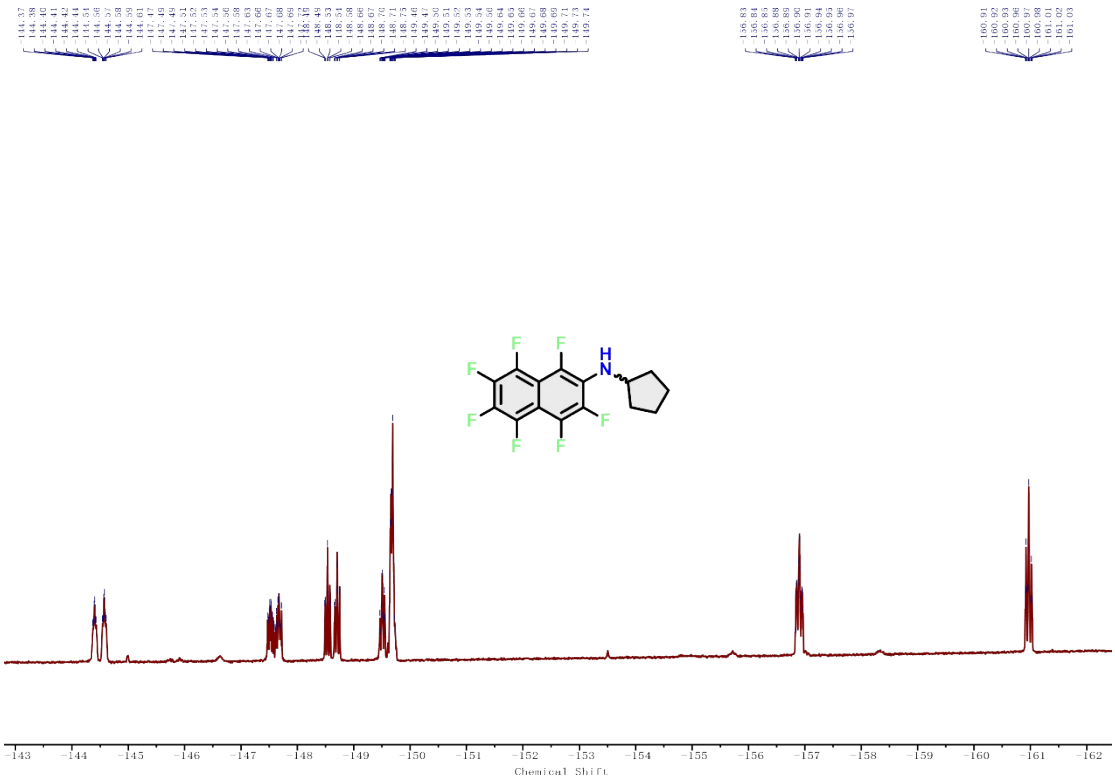

Figure S64. ^{19}F NMR spectra of CPA.

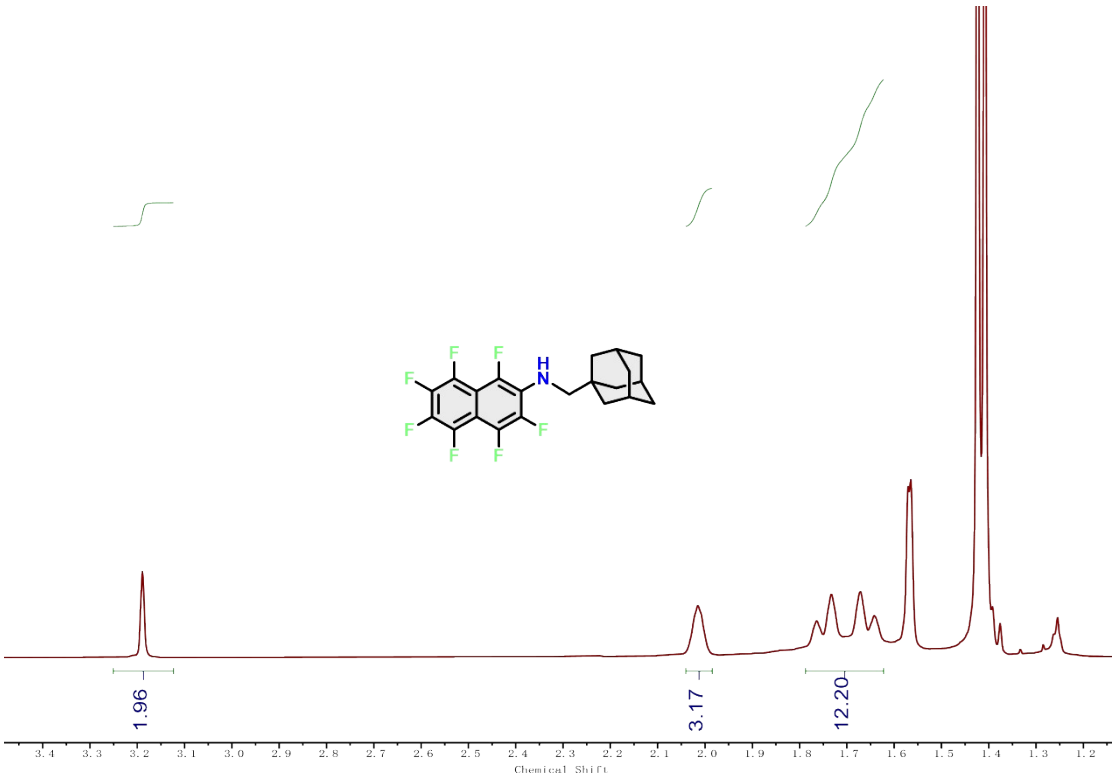

Figure S65. ^{1}H NMR spectra of ADA.

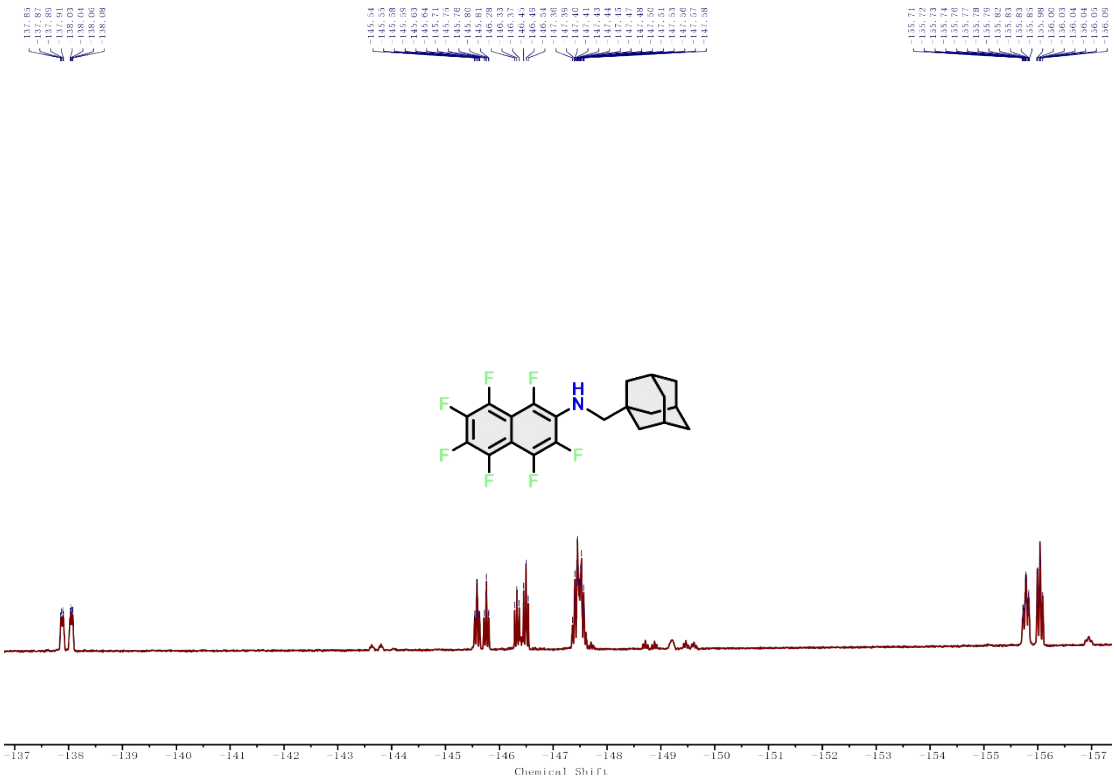

Figure S66. ^{19}F NMR spectra of ADA.

Reference

S1. M. J. Frisch, G. W. Trucks, H. B. Schlegel, G. E. Scuseria, M. A. Robb, J. R. Cheeseman, G. Scalmani, V. Barone, G. A. Petersson, H. Nakatsuji, X. Li, M. Caricato, A. V. Marenich, J. Bloino, B. G. Janesko, R. Gomperts, B. Mennucci, H. P. Hratchian, J. V. Ortiz, A. F. Izmaylov, Gaussian 16, Revision A.03; Gaussian, Inc.: Wallingford, CT, 2016.

S2. T. Lu, F. Chen, *J. Comput. Chem.* **2012**, 33, 580.

S3. W. Ma, X. Li, A. Hao, and P. Xing, *Sci. China. Chem.*, **2024**, 67, 3482.

S4. V. J. Roy, P. P. Sen and S. R. Roy, *Chem. Commun.* 2022, 58, 1776.